

Phase behavior of weakly polydisperse sticky hard spheres:

Perturbation theory for the Percus-Yevick solution

Riccardo Fantoni,^{*} Domenico Gazzillo,[†] and Achille Giacometti[‡]

Istituto Nazionale per la Fisica della Materia and Dipartimento di Chimica Fisica,

Università di Venezia, S. Marta DD 2137, I-30123 Venezia, Italy

Peter Sollich[§]

King's College London, Department of Mathematics, Strand, London WC2R 2LS, U.K.

(Dated: March 23, 2022)

We study the effects of size polydispersity on the gas-liquid phase behaviour of mixtures of sticky hard spheres. To achieve this, the system of coupled quadratic equations for the contact values of the partial cavity functions of the Percus-Yevick solution is solved within a perturbation expansion in the polydispersity, i.e. the normalized width of the size distribution. This allows us to make predictions for various thermodynamic quantities which can be tested against numerical simulations and experiments. In particular, we determine the leading-order effects of size polydispersity on the cloud curve delimiting the region of two-phase coexistence and on the associated shadow curve; we also study the extent of size fractionation between the coexisting phases. Different choices for the size-dependence of the adhesion strengths are examined carefully; the Asakura-Oosawa model of a mixture of polydisperse colloids and small polymers is studied as a specific example.

PACS numbers: 64.60.-i, 64.70.-p, 64.70.Fx, 64.60.Ak

Keywords: Sticky Hard Spheres, polydispersity, perturbation, Percus-Yevick approximation,
phase coexistence

I. INTRODUCTION

In the context of soft matter, a number of systems are known to display a combination of a very steep repulsion and a short range attraction. This includes for instance polymer-coated colloids^{1,2}, globular proteins³ and microemulsions⁴. In spite of the notable differences in the details of the interactions among these systems, most of the common essential features are captured by a paradigmatic model known as the adhesive or sticky hard sphere model. Sticky hard spheres are impenetrable particles of diameters $\{\sigma_i\}$ with an adhesive surface. The simplest way of describing the adhesion properties, in the framework of atomic fluids, was originally proposed by Baxter⁵ in terms of a potential where energy and length scales were combined into a single parameter, thus defining the so-called sticky hard sphere (SHS) potential. Baxter showed that for this model the Ornstein-Zernicke integral equation determining the correlation functions in the liquid state admitted an analytic solution within the Percus-Yevick (PY) approximation. Together with his collaborators, he predicted from this solution (via both the compressibility and the energy routes of liquid state theory) that the model displays a gas-liquid transition^{6,7}. This PY solution was soon extended to mixtures^{8,9,10,11} and has since found a number of interesting applications in the area of colloidal suspensions^{1,2,12,13,14,15}. When studying the phase behavior of such fluids an important issue to deal with is the fact that colloidal particles are generally not identical but may have different characteristics (size, charge, chemical species etc). Often, the distribution of the relevant parameter is effectively continuous and the fluid is then referred to as polydisperse. We will focus in this paper on *size polydispersity*, i.e. a fluid with a distribution of particle

diameters. (A small degree of size polydispersity is in fact required to resolve thermodynamic pathologies which occur in the case of strictly equal-sized, i.e. monodisperse, sticky hard spheres¹⁶.) The particle size distribution is fixed when the particles are synthesized. Thereafter, only the overall density can be modified by adding or removing solvent, while keeping constant all ratios of densities of particles of different size; this traces out a so-called “dilution line” in the phase diagram.

Given the success of the PY closure for the monodisperse SHS model, it is natural to try to extend it to the polydisperse case. Unfortunately, the PY approximation is tractable only for mixtures of a small number of particle species: the case of a binary mixture can be solved analytically¹¹, and for mixtures with a limited number of components (10 or fewer) a numerical solution is feasible¹². The polydisperse case requires one to keep track of an effectively infinite number of particles species, one for each size, and cannot be tackled directly. An alternative, which we have explored in past work, is to use simpler integral equation theories such as the modified Mean Spherical Approximation (mMSA or C0). Between this and the Percus Yevick (PY) approximation⁵ lie a set of increasingly accurate approximations, denoted as C_n with $n = 1, 2, \dots$. They are based on a density expansion of the direct correlation function outside the hard core and can be shown to improve, order by order, the various virial coefficients¹⁷. These C_n approximations *can* be extended to the polydisperse case with relative ease, provided a particular factorization holds for the matrices appearing in the solution of Baxter’s equations. This has allowed us to perform a comprehensive analysis of polydispersity effects on the gas-liquid phase separation¹⁸.

The tractability of the C_n approximations for the polydisperse SHS model does, however, come at the price of lower accuracy. Indeed, for the monodisperse case accurate Monte Carlo simulation data recently published by Miller and Frenkel^{19,20,21} show that the equation of

state of the fluid lies very close to the one derived from the energy route of the PY closure. Both the C0 and C1 approximations, on the other hand, yield precise results only within a rather limited region of the phase diagram, corresponding to high temperatures or low densities¹⁷; see Fig. 1 below.

The above considerations show that another attack on the PY closure for polydisperse SHS fluids is worthwhile in order to get accurate predictions for the gas-liquid phase behavior. Rather than trying to tackle the most general case of a fluid with a potentially wide distribution of particle sizes, which for now remains out of reach, we exploit the idea of Evans²² to treat size polydispersity as a perturbation to the monodisperse phase behavior. For this method to apply, the size distribution only has to be sufficiently narrow but its shape is otherwise arbitrary. Our approach is also of sufficient generality to consider arbitrary dependences of the adhesion strengths on the particle sizes, including those considered in previous work on the C_n approximations^{18,23}. Throughout, we consider gas-liquid phase coexistence only. It has been argued²⁴ that even in the presence of polydispersity this is metastable with respect to phase separation into a colloidal gas and solid. However, the latter may be unobservable on realistic timescales when formation of the polydisperse solid is hindered by large nucleation barriers²⁵ or an intervening kinetic glass transition²⁶; the gas-liquid phase splits we calculate will then control the physically observable behaviour. Even where the kinetics does allow formation of solid phases, the metastable gas-liquid phase behaviour can play a role, e.g. in determining phase ordering pathways²⁷.

The paper is organized as follows. In section II we describe the polydisperse SHS model and discuss various routes for predicting the thermodynamics of this system, comparing their accuracy for the better understood monodisperse case. In the polydisperse setting one needs to model how the strength of the adhesion between two particles depends on their

size; we discuss some possible choices for this in section III. Section IV describes our perturbation expansion of the PY closure for the weakly polydisperse SHS model. We first define the perturbation expansion of the free energy used by Evans (Sec. IV A) and summarize the relevant consequences for two-phase coexistence and the attendant size fractionation effects. The basic equations that need to be solved in order to determine thermodynamic properties within the PY approximation are then described and solved perturbatively (Sec. IV B), while Sec. IV C derives from this, via the energy route, the excess Helmholtz free energy. In section V we evaluate numerically the consequences of polydispersity for two-phase coexistence and fractionation for a number of example scenarios, and compare with alternative approximation schemes. Section VI gives concluding remarks.

II. THE SHS MODEL

The p -component SHS mixture model is made up of Hard Spheres (HS) of different diameters σ_i , $i = 1, 2, \dots, p$, interacting through a particular pair potential defined via the following limit procedure. One starts with a pair interaction potential $\phi_{ij}(r)$ with a hard core extending out to distance $r = \sigma_{ij} = (\sigma_i + \sigma_j)/2$, followed by a square well potential of width $R_{ij} - \sigma_{ij}$:

$$\phi_{ij}(r) = \begin{cases} +\infty & 0 < r < \sigma_{ij} , \\ -\ln \left(\frac{1}{12\tau_{ij}} \frac{R_{ij}}{R_{ij} - \sigma_{ij}} \right) & \sigma_{ij} \leq r \leq R_{ij} , \\ 0 & r > R_{ij} , \end{cases} \quad (1)$$

Here the dimensionless parameter

$$\frac{1}{\tau_{ij}} = \frac{\epsilon_{ij}}{\tau} \geq 0 \quad (2)$$

measures the surface adhesion strength or “stickiness” between particles of species i and j . In Eq. (2) the reduced temperature τ is an unspecified increasing function of the physical temperature T ; the coefficients ϵ_{ij} specify how stickiness depends on which particle species are in contact and are discussed more fully in the next section. The procedure which defines the SHS model then consists in taking the “sticky limit” $R_{ij} \rightarrow \sigma_{ij}$. The logarithm in the initial square well potential (1) is chosen such as to give a simple expression for the Boltzmann factor $\exp[-\phi_{ij}(r)]$, which reduces to a combination of a Heaviside step function and a Dirac delta function in the sticky limit. Here and in the following we measure all energies in units of $k_B T$, to simplify the notation.

A fully polydisperse system is obtained from the above discrete mixture by replacing the molar fractions $x_i = N_i/N$, where N_i is the number of particles of species i and N the total number of particles, with a normalized size distribution function $p(\sigma)$:

$$x_i \longrightarrow p(\sigma) d\sigma .$$

Here $p(\sigma) d\sigma$ is the fraction of spheres with diameter in the interval $(\sigma, \sigma + d\sigma)$. Similarly, given a quantity a_i that depends on the species index one replaces

$$a_i \longrightarrow a(\sigma) ,$$

$$\langle a \rangle = \sum_i x_i a_i \longrightarrow \int_0^\infty a(\sigma) p(\sigma) d\sigma .$$

We next consider the possible methods for predicting the thermodynamic behavior of SHS fluids. As pointed out in the introduction, a good approximation to the effectively exact Monte Carlo (MC) equation of state²⁰ of the *monodisperse* SHS model is obtained by calculating the pressure from the energy route within the PY approximation⁷. In the case of mixtures no comparable Monte Carlo data exists, nor is a direct solution of the PY closure feasible, so that finding a reliable approximation to the equation of state remains an

important open challenge. As described in the introduction, we have tackled this in past work within an approximate theory based on a density expansion of the direct correlation function around the MSA solution^{17,18,23}. Another possible route is thermodynamic perturbation theory. For the Baxter SHS model it is easy to convince oneself that only the scheme proposed by Weeks, Chandler and Anderson (WCA)²⁸ can be applied. We have explored this possibility in the monodisperse case, where Monte Carlo simulations provide reliable reference data. In Fig. 1 we compare the simulation data with the predictions of the Mean-Spherical-Approximation (MSA), the modified Mean-Spherical-Approximation (mMSA) and the C1 approximation (as discussed in¹⁷); the results from the first and second order WCA²⁸ perturbation theory are also shown. It is clear that the mMSA and C1 approximations are fairly reliable for low and intermediate densities, even at low reduced temperatures, while the second-order WCA approximation breaks down already at temperatures significantly above the critical point ($\tau_c \approx 0.11$, depending on the approximation used). The WCA method therefore offers little hope of providing the basis for an accurate equation of state for mixtures. One also sees readily from Fig. 1 that the PY closure provides by far the most accurate of all the approximation methods. This is why we return to the problem of solving the PY approximation for SHS mixtures in this paper.

A major challenge in calculating phase equilibria in polydisperse SHS, or indeed any polydisperse fluid, arises from the fact that its Helmholtz free energy is a functional of the distribution $p(\sigma)$ of the polydisperse attribute²⁹. However, in simple systems or approximations this functional dependence reduces, for the *excess* free energy, to one on a finite number of moments of the distribution. In these cases the free energy is called truncatable^{30,31} and the phase coexistence problem reduces to the solution of a finite number of coupled nonlinear equations. For example, for the size-polydisperse SHS mixture the mMSA

and C1 approximations yield such a truncatable form for the excess free energy involving only three moments ρ_1, ρ_2 and ρ_3 , and the two-phase coexistence problem can easily be solved numerically¹⁸. The relevant moments are defined here including factors of density as

$$\rho_m = \rho \int_0^\infty \sigma^m p(\sigma) d\sigma . \quad (3)$$

for $m = 1, 2, 3$; for later reference we note that ρ_3 is proportional to the hard sphere volume fraction.

When the more accurate PY approximation is used, the presence of polydispersity renders an analytical calculation of the free energy impossible (see section IV B). In addition, even if the free energy could be calculated in closed form, it would almost certainly not have a truncatable form and so predictions for the phase behavior would remain difficult to extract. We therefore propose to consider a small degree of polydispersity as a perturbation²² around the well-understood monodisperse reference system (see²⁹ for an overview of earlier work in this perturbative spirit). Denote by σ_0 a characteristic sphere diameter, which will be taken as the mean diameter of the overall or “parent” size distribution $p^{(0)}(\sigma)$ in the system. We then focus on fluids with a narrow size distribution centered on σ_0 , for which the relative particle size deviations

$$\delta = \frac{\sigma - \sigma_0}{\sigma_0} , \quad (4)$$

are small for all particle sizes σ . Following Evans, we will expand up to second order in these size deviations²². The leading order phase boundary shifts and fractionation effects then turn out to be proportional to s^2 , where $s = [\langle \delta^2 \rangle^{(0)}]^{1/2}$ is the normalized standard deviation – also referred to simply as “polydispersity” – of the parent distribution. Before proceeding to the calculation, we address in the next section the choice of the stickiness coefficients ϵ_{ij} from Eq. (2). These are irrelevant for monodisperse SHS but can have important effects on

the behavior of mixtures as we will see.

III. THE STICKINESS COEFFICIENTS ϵ_{ij}

A. General arguments

At a reduced temperature τ the Boltzmann factor $\exp[-\phi_{ij}(r)]$ for the interaction of two SHS particles depends only on the ratio ϵ_{ij}/τ (and, of course, on σ_{ij}). Physically, the stickiness coefficients ϵ_{ij} represent dimensionless adhesion energies between pairs of particles identified by the species indices i and j . (We revert to the notation for the discrete mixture here; the same considerations obviously apply to the polydisperse system.) The ϵ_{ij} have no analogue in the monodisperse case, where only the reduced temperature τ features and ϵ can be set to unity. For (discrete or polydisperse) mixtures, on the other hand, one needs to make an appropriate choice for the dependence $\epsilon_{ij} = \mathcal{F}(\sigma_i, \sigma_j)$ of the stickiness coefficients on the particle sizes. We discuss possibilities for this choice in this section.

Clearly the appropriate form of the function $\mathcal{F}(\sigma_i, \sigma_j)$ will depend on the kind of physical problem one is studying. Nevertheless, it should satisfy some general requirements: (i) Adhesion should be a purely pairwise property, and so \mathcal{F} should depend only on σ_i and σ_j as anticipated by our notation; \mathcal{F} must clearly also be symmetric under interchange of σ_i and σ_j . (ii) Since the ϵ_{ij} are dimensionless, so must \mathcal{F} be. If it does not contain a separate lengthscale, it is therefore a homogeneous function of degree zero in (σ_i, σ_j) . The latter case is interesting because it can be seen as the sticky limit of a scalable (i.e. purely size-polydisperse) interaction²², where by definition $\phi_{ij}(r)$ remains unchanged when r , σ_i and σ_j are all scaled by a common factor. (The square well potential of Eq. (1) can be put into this form by choosing $R_{ij} = \sigma_{ij}[1 + 1/(A\epsilon_{ij} - 1)]$; the sticky limit is obtained by letting

$A \rightarrow \infty$.) The presence of pure size-polydispersity has important simplifying effects on the phase behavior^{32,33} which we discuss further in Sec. V below. (iii) If the adhesion depends on the surface area of the spheres one might expect \mathcal{F} to depend on ratios of homogeneous functions of degree two in (σ_i, σ_j) . (iv) If the adhesive interaction vanishes when at least one of the two particles i and j degenerates to a point we need to require $\lim_{\sigma_i \rightarrow 0} \mathcal{F}(\sigma_i, \sigma_j) = 0$; the limit for $\sigma_j \rightarrow 0$ is then also zero, by the symmetry of \mathcal{F} .

In Ref.¹⁸ plausibility and convenience arguments were adduced to suggest the following choices for the quantities ϵ_{ij} :

$$\epsilon_{ij} = \mathcal{F}(\sigma_i, \sigma_j) = \begin{cases} \sigma_0^2 / \sigma_{ij}^2 & \text{Case I ,} \\ \sigma_i \sigma_j / \sigma_{ij}^2 & \text{Case II ,} \\ 1 & \text{Case IV ,} \\ \sigma_0 / \sigma_{ij} & \text{Case V .} \end{cases} \quad (5)$$

Here σ_0 is a characteristic reference length for the sizes, taken as above to be the parental mean diameter. In the forms originally suggested¹⁸, this length was chosen as a moment of the size distribution, $\langle \sigma^n \rangle^{1/n}$ with either $n = 1$ or 2 . (Case I here corresponds to cases I and III in Ref.¹⁸; we have kept the original numbering for the remaining cases II, IV and V for ease of reference.) However, this identification has the drawback of introducing many-body effects into the pair potential, as the moments $\langle \sigma^n \rangle$ depend upon the thermodynamic state of the fluid, and in particular on the concentrations of *all* particle species. This is why we have chosen the fixed reference length σ_0 above, consistent with the notion of a purely pairwise interaction. Numerically the actual choice of σ_0 turns out to have only very minor effects; this can be shown by calculations (not reproduced here) comparing case I (with fixed σ_0) with case III from¹⁸, obtained by replacing $\sigma_0 \rightarrow \langle \sigma^2 \rangle^{1/2}$.

The form of the $1/\sigma_{ij}^2$ denominator for cases I and II in Eq. (5) is forced by technical

constraints detailed in Ref.¹⁸, but these still leave some flexibility in the choice of numerator; cases I and II assume respectively a mean-field-like and a decoupled dependence between stickiness and size. Case IV corresponds to the choice of constant coefficients (independent of particle sizes), while case V was selected in Ref.¹⁸ specifically to permit analytical solution within the C1 closure. Note that not all four cases have all of the properties (ii–iv) listed above as possible requirements. E.g. only cases II and IV are homogeneous functions of (σ_i, σ_j) as required by (ii) when no additional lengthscale such as σ_0 is involved; they are therefore purely size-polydisperse. The properties (iii) and (iv) hold only for case II. It can be argued³⁴ that the dependence on $\sigma_i\sigma_j/\sigma_{ij}^2$ assumed in case II is quite generic for solutions of colloids, micelles or globular proteins, at least in the high-temperature regime where a linearized approximation for the Boltzmann factor is sufficient. While this favors case II, for phase coexistence we are interested in lower temperatures where it is less clear which case is physically more appropriate; we will therefore include all four cases in our analysis.

For our perturbative analysis we only need to know the coefficients in the expansion of the ϵ_{ij} around the typical particle size $\sigma_i = \sigma_j = \sigma_0$, up to quadratic order in the relative particle size deviations $\delta_i = (\sigma_i - \sigma_0)/\sigma_0$:

$$\epsilon_{ij} = \epsilon_0 + \epsilon_{1a}(\delta_i + \delta_j) + \epsilon_{2a}\delta_i\delta_j + \epsilon_{2b}(\delta_i^2 + \delta_j^2) + \dots \quad (6)$$

The coefficients $\epsilon_0, \epsilon_{1a}, \epsilon_{2a}, \epsilon_{2b}$ of this expansion are given in Table I for the four cases listed above. Note that $\epsilon_0 = 1$ always so that in the monodisperse limit the ϵ_{ij} are irrelevant as they should be.

B. Stickiness coefficients for the Asakura-Oosawa model

So far we have considered choices for the stickiness coefficients suggested by rather general arguments. One may wonder whether the ϵ_{ij} can be derived more directly from a physical picture. We shall pursue this here for the well-known Asakura-Oosawa model of colloid-polymer mixtures, which for small polymers leads to a short-ranged attractive depletion potential acting between the colloids³⁵. We shall show that, while a formal sticky limit cannot be taken in general when colloids of different sizes are present, an effective SHS model can still be derived when the polymer size is small but kept nonzero. This then simplifies further in the perturbative approach for weak polydispersity adopted here.

Consider two colloidal particles represented by impenetrable spheres of diameter σ_i and σ_j immersed in a solution of non-interacting polymers. Within the Asakura-Oosawa model, the polymers are simplified to spheres of diameter ξ which can fully penetrate each other but have a hard sphere interaction with the colloids. It is well known that such a system develops an entropically driven effective attraction between the colloidal particles. This arises due to a reduction in the volume from which the polymers are excluded when the exclusion zones around the colloids overlap (see Fig. 2). This overlap volume as a function of the distance r between the sphere centers is

$$\mathcal{V}_{\text{ov}}(r) = \frac{\pi}{12} \left[r^3 - 6(R_i^2 + R_j^2)r + 8(R_i^3 + R_j^3) - 3(R_i^2 - R_j^2)^2 \frac{1}{r} \right] \theta(\sigma_{ij} + \xi - r) \quad (7)$$

where $R_k = (\sigma_k + \xi)/2$ and only distances $r > \sigma_{ij}$ are allowed because of the hard colloid-colloid repulsion. The effective colloid-colloid attraction induced by the presence of the polymers is then just the overlap volume times the polymer osmotic pressure^{35,36}, giving the

overall AO interaction potential

$$\phi_{ij}^{\text{AO}}(r) = \begin{cases} +\infty & 0 < r < \sigma_{ij} , \\ -\rho_p \mathcal{V}_{\text{ov}}(r) & \sigma_{ij} \leq r < \sigma_{ij} + \xi , \\ 0 & r \geq \sigma_{ij} + \xi , \end{cases} \quad (8)$$

This expression can be obtained formally by integrating out the polymer degrees of freedom from the partition function at fixed polymer chemical potential. The latter is conveniently parametrized by the density ρ_p of polymers in a reservoir connected to the system; because the polymers are taken as ideal, their osmotic pressure is then $k_B T \rho_p$ and the $k_B T$ is absorbed by our choice of units. The effective colloid-colloid interaction will in general contain also many-body terms, but these vanish in the limit of small polymers (for monodisperse colloids the condition is $\xi < 0.1547\sigma_0$) that we are interested in.

To map to an equivalent SHS potential, which should be physically reasonable for small polymer-to-colloid size ratio ξ/σ_0 , one equates the corresponding second virial coefficients. The hard core makes the same contribution ($B_{2,\text{HS}}^{ij} = 2\pi\sigma_{ij}^3/3$) in the SHS and the original AO potential, so one can focus on the normalized deviation of the second virial coefficient from this HS value,

$$\begin{aligned} \Delta B_{2,\text{AO}}^{ij} &= \frac{B_{2,\text{AO}}^{ij} - B_{2,\text{HS}}^{ij}}{B_{2,\text{HS}}^{ij}} \\ &= \frac{3}{\sigma_{ij}^3} \int_{\sigma_{ij}}^{\sigma_{ij}+\xi} \left[1 - e^{-\phi_{ij}^{\text{AO}}(r)} \right] r^2 dr . \end{aligned}$$

For the SHS potential this quantity equals $-1/(4\tau_{ij})$, so the stickiness parameters in the mapped SHS system are assigned as

$$\frac{1}{12\tau_{ij}} = \frac{1}{\sigma_{ij}^3} \int_{\sigma_{ij}}^{\sigma_{ij}+\xi} \left[e^{-\phi_{ij}^{\text{AO}}(r)} - 1 \right] r^2 dr . \quad (9)$$

We now proceed to simplify this expression for small ξ ; in the limit $\xi \rightarrow 0$, the original AO model should become fully equivalent to the mapped SHS system. We will see that

for mixtures of colloids of different sizes this strict mathematical limit cannot be taken consistently; nevertheless, as long as ξ/σ_0 is small, we expect the SHS mixture to give a reasonably accurate description of the underlying AO model.

To simplify Eq. (9) we change integration variable from r to $z = (r - \sigma_{ij})/\xi$, expand the attractive tail of the AO potential in ξ as

$$-\phi_{ij}^{\text{AO}}(z) = \frac{\pi}{4}\rho_p\xi^2\frac{\sigma_i\sigma_j}{\sigma_{ij}}(z-1)^2 + O(\xi^3) . \quad (10)$$

and retain only the leading term. Similarly approximating $r^2 = (\sigma_{ij} + \xi z)^2 = \sigma_{ij}^2 + O(\xi)$ yields

$$\frac{1}{12\tau_{ij}} = \frac{\xi}{\sigma_{ij}} \int_0^1 \left[e^{\gamma_{ij}(1-z)^2} - 1 \right] dz = \frac{\xi}{\sigma_{ij}} \left[\frac{1}{2} \sqrt{\frac{\pi}{\gamma_{ij}}} \text{erfi}(\sqrt{\gamma_{ij}}) - 1 \right] \quad (11)$$

where

$$\gamma_{ij} = \frac{\pi}{4}\rho_p\xi^2\frac{\sigma_i\sigma_j}{\sigma_{ij}}$$

is the value of the attractive potential at contact and $\text{erfi}(z) = \text{erf}(iz)/i$ is the imaginary error function. Because of the prefactor ξ/σ_{ij} in Eq. (11), γ_{ij} has to grow as ξ decreases if we want to keep τ_{ij} finite. For large argument the error function behaves as $\text{erfi}(z) = e^{z^2}[1/z + O(1/z^3)]/\sqrt{\pi}$ and so

$$\frac{1}{12\tau_{ij}} \approx \frac{\xi}{\sigma_{ij}} \frac{e^{\gamma_{ij}}}{2\gamma_{ij}} = \frac{2}{\pi\rho_p\xi\sigma_i\sigma_j} e^{\frac{\pi}{4}\rho_p\xi^2\frac{\sigma_i\sigma_j}{\sigma_{ij}}} .$$

A nonzero limit value of τ_{ij} for $\xi \rightarrow 0$ thus requires that γ_{ij} grows logarithmically as $\gamma_{ij} = \ln(\sigma_{ij}/\xi)$ to leading order. The corresponding polymer reservoir density, likewise to leading order, goes as

$$\rho_p = \frac{4}{\pi} \frac{\sigma_{ij}}{\sigma_i\sigma_j} \frac{\ln(\sigma_0/\xi)}{\xi^2} . \quad (12)$$

The dominant dependence $\rho_p \propto \xi^{-2}$ in this expression arises because the value of the AO potential at contact scales as $\rho_p\xi^2$; the additional logarithmic factor increases this interaction

strength to compensate for the decreasing range of the attraction as $\xi \rightarrow 0$. Note that even though the polymer density diverges, the polymers do in fact become very dilute as one sees from the (reservoir) volume fraction $\eta_p = (\pi/6)\rho_p\xi^3 \sim \xi \ln(\sigma_0/\xi)$ occupied by the polymer spheres.

For monodisperse colloids, the above procedure produces an unambiguous sticky limit for $\xi \rightarrow 0$. The explicit form of Eq. (12) shows, however, that this limit cannot be taken straightforwardly for mixtures: the prefactors $\sigma_{ij}/(\sigma_i\sigma_j)$ of the required leading order divergences of the polymer density are incompatible with each other for different pairs of particle species. In other words, if the ξ -dependence of the polymer density is chosen to keep one specific τ_{ij} finite and nonzero, then the others would either tend to zero or grow to infinity in the sticky limit. The example of a binary mixture illustrates this. Suppose that $\sigma_1 > \sigma_2$ and that the polymer density is tuned to keep the τ_{11} finite. Then $1/\tau_{12}$ and $1/\tau_{22}$ would both tend to zero for $\xi \rightarrow 0$ so that all interactions involving particles of species 2 become purely HS-like, without any attractive contributions (this is system B studied in²³).

In the absence of a strict sticky limit, we will content ourselves with applying the mapping (11) for small but nonzero polymer-to-colloid size ratios ξ/σ_0 . The properties of the resulting SHS mixture should then still give a good approximation to those of the original AO model. In the perturbative setting of this paper we can then expand Eq. (11) in the small relative deviations $\delta_i = (\sigma_i - \sigma_0)/\sigma_0$ of the particle sizes from the parental mean. In the decomposition $1/\tau_{ij} = \epsilon_{ij}/\tau$ of Eq. (2) we fix the scale of the ϵ_{ij} by requiring as before that $\epsilon_{ij} = 1$ for particles of the reference size $\sigma_i = \sigma_j = \sigma_0$. This gives

$$\frac{1}{\tau} = \frac{12\xi}{\sigma_0} \left[\frac{1}{2} \sqrt{\frac{\pi}{\gamma}} \text{erfi}(\sqrt{\gamma}) - 1 \right] \approx \frac{6\xi}{\sigma_0} \frac{e^\gamma}{\gamma} \quad (13)$$

for the reduced temperature, where

$$\gamma = \frac{\pi}{4} \rho_p \xi^2 \sigma_0 .$$

The second, approximate equality in Eq. (13) holds for large γ as before. To find the perturbative expansion of the stickiness coefficients ϵ_{ij} , we note first that the potentials at contact expand as

$$\gamma_{ij} = \gamma \left[1 + \frac{1}{2}(\delta_i + \delta_j) + \frac{1}{2}\delta_i\delta_j - \frac{1}{4}(\delta_i^2 + \delta_j^2) \right]$$

Since the erfi in Eq. (11) grows at most as $\exp(\gamma_{ij})$, a second order Taylor expansion will give an accurate approximation as long as the perturbations in γ_{ij} are $\ll 1$. This requires $\delta_i \ll 1/\gamma$, which then automatically enforces $\delta_i \ll 1$ since we expect γ to be at least of order unity for the mapping to a SHS mixture to make sense. Under these conditions one then has a valid perturbation expansion of the ϵ_{ij} . The coefficients defined in Eq. (6) are found as $\epsilon_0 = 1$ (by our choice of τ) and

$$\epsilon_1 = \frac{-1 + g_1}{2}, \quad \epsilon_{2a} = \frac{1 + g_2}{2}, \quad \epsilon_{2b} = \frac{1 - 2g_1 + g_2}{4}$$

where

$$g_1 = \frac{e^\gamma - 1}{\sqrt{\pi/\gamma} \operatorname{erfi}(\sqrt{\gamma}) - 2} - \frac{1}{2}$$

$$g_2 = \frac{[3 + e^\gamma(2\gamma - 3)]/4}{\sqrt{\pi/\gamma} \operatorname{erfi}(\sqrt{\gamma}) - 2} + \frac{3}{8} .$$

From Eq. (13) one sees that the reduced temperature is set by the contact potential γ , which itself is proportional to the polymer reservoir density. Unlike the more ad-hoc choices of Eq. (5), the expansion of the ϵ_{ij} in terms of the δ_i depends on the reduced temperature τ , via γ . For large γ one can use the leading order approximations $g_1 \approx \gamma - 1$, $g_2 \approx (\gamma^2 - 2\gamma + 1)/2$ to evaluate this dependence. However, since typical values of γ are only logarithmically large in σ_0/ξ it is generally safer to work with the full expressions.

IV. PERTURBATION THEORY FOR THE POLYDISPERSE PY CLOSURE

In this section we come to the core of our analysis. We first review Evans' perturbative framework for slightly polydisperse systems. To apply this to the PY approximation for SHS mixtures we will need the perturbative expansion of certain correlation function values at contact; from these we can then finally find the excess free energy.

A. Evans' perturbative expansion

The starting point for an analysis of the phase behavior of polydisperse systems is the excess free energy density. In general this is a functional of the size distribution $p(\sigma)$ in the system. It is also a function of the particle density ρ , and of temperature; we do not write the latter explicitly below. For slightly polydisperse systems it is expedient to switch from σ to the relative deviations δ from the reference size σ_0 . By the fundamental assumption of a narrow size distribution, the δ are small quantities, and one can expand the excess free energy density f^{ex} , measured again in units of $k_{\text{B}}T$, in terms of moments of $p(\delta)$ ²²:

$$f^{\text{ex}}(\rho, [p(\delta)]) = f_0^{\text{ex}}(\rho) + \rho a(\rho) \langle \delta \rangle + \rho b(\rho) \langle \delta^2 \rangle + \rho c(\rho) \langle \delta^3 \rangle + \dots \quad (14)$$

Here terms up to second order in δ have been retained; these give the leading effects on the phase boundaries²². Our functions a, b, c differ by factors of ρ from those defined in Ref.²², so that e.g. a equals Evans' A/ρ ; this simplifies the statement of Eqs. (15-17) below. The leading term f_0^{ex} is the excess free energy density of the monodisperse reference system where all particles have $\delta = 0$.

Given the above expansion of the excess free energy, the conditions for two-phase equilibria of the near-monodisperse fluid can be solved perturbatively²². We briefly recall the main results. The fluid is initially in a parent phase of density $\rho^{(0)}$, with a parent size distribution

function $p^{(0)}(\delta)$, where $\langle\delta\rangle^{(0)} = 0$ by our choice of the reference size σ_0 as the parental mean. In order to lower its free energy, the fluid can split into two daughter phases of densities $\rho^{(1)}$ and $\rho^{(2)}$, with distribution functions $p^{(1)}(\delta)$ and $p^{(2)}(\delta)$ which are in general different from the parent distribution, a phenomenon referred to as *fractionation*²⁹. The densities and size distributions can be worked out perturbatively at any point inside the coexistence region²²; we focus on the properties at the *onset* of phase coexistence, which are most easily accessible experimentally.

Suppose the system is just starting to phase separate, with all of the volume except for an infinitesimal fraction still occupied by phase 1, with density $\rho^{(1)}$. Conservation of particle number then requires that $p^{(1)}(\delta) = p^{(0)}(\delta)$, i.e. the size distribution in this *cloud* phase equals the parent. The coexisting *shadow* phase 2, on the other hand, will generally have $p^{(2)}(\delta) \neq p^{(0)}(\delta)$. Evans²² showed that the cloud and shadow densities, $\rho^{(1)} = \rho_0^{(1)} + \delta\rho^{(1)}$ and $\rho^{(2)} = \rho_0^{(2)} + \delta\rho^{(2)}$, are shifted from their monodisperse values $\rho_0^{(1)}$ and $\rho_0^{(2)}$ by

$$\delta\rho^{(1)} = -s^2\rho_0^{(1)}\kappa(\rho_0^{(1)})\left[(\rho_0^{(1)})^2b'(\rho_0^{(1)}) + \frac{(\Delta a)^2 + 2\Delta b}{2\Delta(1/\rho)}\right] \quad (15)$$

$$\delta\rho^{(2)} = -s^2\rho_0^{(2)}\kappa(\rho_0^{(2)})\left[(\rho_0^{(2)})^2b'(\rho_0^{(2)}) + \frac{(\Delta a)^2 + 2\Delta b}{2\Delta(1/\rho)} + (\rho_0^{(2)})^2a'(\rho_0^{(2)})\Delta a\right] \quad (16)$$

Here $a' \equiv \partial a/\partial\rho$, $b' \equiv \partial b/\partial\rho$ and $\kappa(\rho) = 1/[\rho + \rho^2(\partial/\partial\rho)^2 f_0^{\text{ex}}(\rho)]$ is the isothermal compressibility of the monodisperse reference system. The shorthand Δ indicates differences between the two monodisperse reference phases, e.g. $\Delta a = a(\rho_0^{(1)}) - a(\rho_0^{(2)})$. Finally, recall that s is the parent polydispersity: the phase boundary shifts are to leading order quadratic in s .

It is worth noting that Eqs. (15,16) are not symmetric in $\rho_0^{(1)}$ and $\rho_0^{(2)}$; by interchanging the two densities one therefore obtains a different cloud-shadow pair. Physically, this corresponds to approaching the onset of phase separation from low or high densities; in a polydisperse system the coexisting phases are different in the two situations since only the

respective majority (cloud) phase has the parental size distribution. The size distribution in the corresponding *shadow* reads, to leading order in δ^{22} ,

$$p^{(2)}(\delta) = p^{(0)}(\delta)[1 + (\Delta a)\delta] . \quad (17)$$

Overall, the monodisperse binodal delimiting the coexistence region splits into separate cloud and shadow curves, which intersect in the critical point²⁹. Quantitative information about the critical region is not accessible within the perturbative expansion of Eqs. (15,16), however, since the compressibility κ diverges as the critical point is approached.

The above summary shows that knowledge of the functions a , b and c is sufficient to calculate the leading order phase boundary shifts and fractionation effects for weakly polydisperse systems. In the next two subsections we calculate these functions for the SHS mixture within the PY approximation.

B. Perturbative analysis of the PY closure

To lighten the notation in the rest of the paper, we make all densities dimensionless by measuring them in units of v_0^{-1} , where

$$v_0 = (\pi/6)\sigma_0^3$$

is the volume of a particle with the reference diameter. The third moment ρ_3 defined in Eq. (3) is then identical to the hard sphere volume fraction η . We also measure all particle sizes σ in terms of σ_0 , so that the relation between σ and the fractional deviation from the parental mean diameter becomes simply $\sigma = 1 + \delta$. In the monodisperse case, where all particles have $\delta = 0$, all moments (3) are then identical and equal to the density ρ (which also equals the volume fraction η). Finally, for notational simplicity we again revert

temporarily to the case of a discrete p -component SHS mixture; the final results will be expressed in terms of averages over the size distribution and so generalize immediately to fully polydisperse systems.

In order to extract the desired thermodynamic quantities from the PY closure, the following set of $p(p+1)/2$ coupled quadratic equations needs to be solved first¹⁰,

$$L_{ij} = \alpha_{ij} + \beta_{ij} \sum_m x_m \left[\frac{1}{12} L_{im} L_{jm} - \frac{1}{2} (L_{im} \phi_{mj} + L_{jm} \phi_{mi}) \right], \quad i, j = 1, 2, \dots, p \quad (18)$$

where the unknowns are

$$L_{ij} = \frac{y_{ij}(\sigma_{ij}) \sigma_{ij}^2 \epsilon_{ij}}{\tau}.$$

Here $y_{ij}(\sigma_{ij})$ is the partial cavity function at contact which is proportional to the probability of finding a particle of species j touching any given particle of species i . In Eq. (18) the coefficients α_{ij} , β_{ij} , and ϕ_{ij} are given by

$$\alpha_{ij} = y_{ij}^{\text{HS}}(\sigma_{ij}) \sigma_{ij}^2 \epsilon_{ij} / \tau, \quad (19)$$

$$\beta_{ij} = \rho \sigma_{ij} \epsilon_{ij} / \tau, \quad (20)$$

$$\phi_{ij} = \sigma_i \sigma_j / \Delta. \quad (21)$$

Here the quantities

$$y_{ij}^{\text{HS}}(\sigma_{ij}) = \frac{1}{\Delta} + \frac{3}{2} \frac{\rho_2}{\Delta^2} \frac{\sigma_i \sigma_j}{\sigma_{ij}} \quad (22)$$

are the PY partial cavity functions at contact for the HS fluid (to which the SHS fluid reduces at infinite reduced temperature τ) and we abbreviate $\Delta = 1 - \eta$, with $\eta \equiv \rho_3$ the HS packing fraction as before. Notice that all four sets of coefficients L_{ij} , α_{ij} , β_{ij} , and ϕ_{ij} are symmetric under exchange of the species indices i and j .

For one-component fluids, the system (18) reduces to a single quadratic equation. Baxter⁵ showed that only the smaller of the two real solutions (provided such solutions exist at all)

is physically significant; it is given explicitly in Eq. (24) below. For true mixtures ($p > 1$), explicit solution of the rather complicated system (18) of algebraic equations is feasible at best numerically (except for special cases^{12,23}) and is the computational bottleneck of the PY solution. For large p , and certainly for the polydisperse limit $p \rightarrow \infty$, it is impossible in practice. However, progress can be made for near-monodisperse fluids by solving (18) perturbatively. The L_{ij} will generically depend on the reduced temperature τ , the overall number density ρ , the sizes σ_i and σ_j of the particles at contact, and all the molar fractions x_i (or their polydisperse analogue, the size distribution $p(\delta)$). For small δ_i we can therefore expand to quadratic order as

$$L_{ij} = L_0 + L_{1a}(\delta_i + \delta_j) + L_{1b}\langle\delta\rangle + L_{2a}\delta_i\delta_j + L_{2b}(\delta_i^2 + \delta_j^2) + L_{2c}\langle\delta\rangle(\delta_i + \delta_j) + L_{2d}\langle\delta\rangle^2 + L_{2e}\langle\delta^2\rangle. \quad (23)$$

The idea now is to insert this expansion, and the analogous expansions of the known coefficients α_{ij} , β_{ij} and ϕ_{ij} , into the r.h.s. of Eq. (18). Having done this, one re-expands to quadratic order in δ_i , δ_j , δ_m and $\langle\delta\rangle$, and to linear order in $\langle\delta^2\rangle$. Finally one replaces $\sum_m x_m = 1$ and $\sum_m x_m \delta_m^n = \langle\delta^n\rangle$ for $n = 1, 2$. Comparing terms of the same form on the left and right of Eq. (18) one then finds a relatively simple set of equations for the coefficients L_0, \dots, L_{2e} , as outlined in the Appendix. To order zero in polydispersity one of course retrieves Baxter's original quadratic equation (Eq. (A5)), whose physically relevant solution is

$$L_0 = \frac{\alpha_0}{\frac{1}{2} \left[1 + \frac{\beta_0}{\Delta_0} + \sqrt{\left(1 + \frac{\beta_0}{\Delta_0}\right)^2 - \frac{\beta_0 \alpha_0}{3}} \right]}, \quad (24)$$

where $\Delta_0 = 1 - \rho$ is the value of Δ in a monodisperse system with density ρ . Since we are perturbing around the physical solution (24) for the monodisperse case, the results we find

for slightly polydisperse mixtures will automatically have the correct physical behavior. In a non-perturbative solution, one would need to check separately that the solution branch with the correct low-density limit $L_{ij} \rightarrow \sigma_{ij}^2/\tau_{ij}$ has been selected; this condition arises since $y_{ij}(\sigma_{ij}) \rightarrow 1$ at low density.

The conditions imposed by Eq. (18) for the higher order expansion coefficients L_{1a}, \dots, L_{2e} turn out to be *linear* and can be straightforwardly solved order by order; see the Appendix. The region in the density-temperature plane where Eq. (18) has no physical solution therefore remains as in the monodisperse case, being delimited by $\rho_- < \rho < \rho_+$ with

$$\rho_{\pm} = \frac{1 - 6(\tau - \tau^2) \pm \sqrt{1 - 12\tau + 18\tau^2}}{5 - 12\tau + 6\tau^2}. \quad (25)$$

for $\tau < (2 - \sqrt{2})/6$. This is clearly an artifact of our finite-order perturbation theory, given that we know from numerical solutions of Eq. (18) that the region where solutions exist does change with increasing polydispersity¹². To reproduce this effect within our approach, a resummation of the perturbation theory to all orders would be needed.

C. Excess free energy

Given the perturbative expansion for L_{ij} , we can determine the free energy of weakly polydisperse SHS mixtures in the PY approximation. There are three known thermodynamic routes (via the energy, compressibility, and virial) that could potentially be used¹¹. We focus on the one that gives the most reliable equation of state for the monodisperse system (see Fig. 1), i.e. the energy route. It predicts in general for the τ -derivative of the excess free energy density

$$\frac{\partial f^{\text{ex}}}{\partial \tau} = \frac{\rho^2}{\tau} \sum_{ij} x_i x_j \sigma_{ij} L_{ij}$$

Inserting the expansion (23) of L_{ij} and re-expanding to quadratic order yields

$$\frac{\partial f^{\text{ex}}}{\partial \tau} = \frac{\rho^2}{\tau} [\Gamma_0 + \Gamma_1 \langle \delta \rangle + \Gamma_2 \langle \delta \rangle^2 + \Gamma_3 \langle \delta^2 \rangle] ,$$

where

$$\Gamma_0 = L_0 ,$$

$$\Gamma_1 = L_0 + 2L_{1a} + L_{1b} ,$$

$$\Gamma_2 = L_{1a} + L_{1b} + L_{2a} + 2L_{2c} + L_{2d} ,$$

$$\Gamma_3 = L_{1a} + 2L_{2b} + L_{2e} .$$

We can then integrate from the desired value of τ to the hard-sphere limit $\tau \rightarrow \infty$ to find

$$\Delta f^{\text{ex}} \equiv f^{\text{ex}} - f_{\text{HS}}^{\text{ex}} = \Delta f_0^{\text{ex}} + \Delta f_1^{\text{ex}} \langle \delta \rangle + \Delta f_2^{\text{ex}} \langle \delta \rangle^2 + \Delta f_3^{\text{ex}} \langle \delta^2 \rangle ,$$

where

$$\Delta f_i^{\text{ex}} = -\rho^2 \int_{\tau}^{\infty} \Gamma_i(\tau') \frac{d\tau'}{\tau'} , \quad i = 0, 1, 2, 3 .$$

and $f_{\text{HS}}^{\text{ex}}$ is the excess free energy density of the HS fluid. For the latter we use the standard Boublik³⁷, Mansoori, Carnahan, Starling, and Leland³⁸ (BMCSL) expression³⁹. Expanded to second order in polydispersity this reads

$$f_{\text{HS}}^{\text{ex}} = f_{\text{HS},0}^{\text{ex}} + f_{\text{HS},1}^{\text{ex}} \langle \delta \rangle + f_{\text{HS},2}^{\text{ex}} \langle \delta \rangle^2 + f_{\text{HS},3}^{\text{ex}} \langle \delta^2 \rangle ,$$

where

$$\begin{aligned} f_{\text{HS},0}^{\text{ex}} &= \frac{\rho^2(4-3\rho)}{\Delta_0^2} , \\ f_{\text{HS},1}^{\text{ex}} &= \frac{6\rho^2(2-\rho)}{\Delta_0^3} , \\ f_{\text{HS},2}^{\text{ex}} &= 3\rho \left[\frac{\rho(1+2\rho)(3+\rho-\rho^2)}{\Delta_0^4} + \ln \Delta_0 \right] , \\ f_{\text{HS},3}^{\text{ex}} &= 3\rho \left[\frac{\rho(1+3\rho-2\rho^2)}{\Delta_0^3} - \ln \Delta_0 \right] . \end{aligned}$$

Altogether we therefore have, for the perturbative expansion (14) of the excess free energy density of the SHS mixture,

$$\begin{aligned}
 f_0^{\text{ex}} &= f_{\text{HS},0}^{\text{ex}} + \Delta f_0^{\text{ex}}, \\
 a\rho &= f_{\text{HS},1}^{\text{ex}} + \Delta f_1^{\text{ex}}, \\
 b\rho &= f_{\text{HS},3}^{\text{ex}} + \Delta f_3^{\text{ex}}, \\
 c\rho &= f_{\text{HS},2}^{\text{ex}} + \Delta f_2^{\text{ex}}.
 \end{aligned} \tag{26}$$

With these results we can now proceed to apply Evans' general results to study cloud and shadow curves and fractionation effects in polydisperse SHS mixtures.

Inspection of the lengthy explicit expressions for a , b and c shows that the dependence on the stickiness expansion coefficients ϵ_{1a} , ϵ_{2a} , ϵ_{2b} is in fact rather simple. For a one finds the form

$$a = a_0 + \epsilon_{1a} a_1, \tag{27}$$

with a_0 and a_1 functions of ρ and τ only. This is reasonable since a is the coefficient of a first order (in δ) term in the excess free energy, and should therefore only depend on the expansion of the ϵ_{ij} to the same order. The function b involves in addition terms proportional to ϵ_{1a}^2 and ϵ_{2b} , while the remaining coefficient ϵ_{2a} occurs only in the function c . Since c does not feature in the expressions for the phase boundary shifts or fractionation effects to $O(s^2)$, all results we show below are therefore independent of ϵ_{2a} .

V. PHASE BEHAVIOR

In this section we show our results for the phase behavior of polydisperse SHS mixtures. We will explore the various choices of stickiness coefficients discussed in Sec. III, i.e. cases I, II, IV and V as well as the AO model for small values of the polymer-to-colloid size ratio.

The first subsection has the main results from our perturbation theory in polydispersity for the PY closure; in Sec. VB we then compare these predictions with those from other approximation schemes.

A. PY closure

We start by recalling in Fig. 3 the phase diagram of the monodisperse SHS fluid as obtained within the PY approximation and using the energy route to thermodynamics. Along with the binodal we show the spinodal, where the curvature of the free energy vanishes and a homogeneous phase becomes unstable to local density fluctuations, and the region (25) where Baxter's PY equation has no physical solution. Here and in the following we use on the x -axis the volume fraction η rather than the density ρ . In our units, these two quantities are identical for monodisperse systems, but differ to order s^2 in the presence of size polydispersity. For parent phases specifically, Eq. (A4) gives $\eta^{(0)} = \rho^{(0)}(1 + 3s^2)$ to quadratic order. Cloud phases, which share the parental size distribution, have similarly $\rho^{(1)} = \rho_0^{(1)}(1 + 3s^2) + \delta\rho^{(1)}$, while for shadow phases one finds using Eq. (17) that $\rho^{(2)} = \rho_0^{(2)}[1 + 3(1 + \Delta a)s^2] + \delta\rho^{(2)}$ ²².

To get some initial intuition for the effects of polydispersity, it is useful to consider first the single-phase equation of state. Fig. 4 shows plots of the dimensionless pressure against volume fraction at several values of the polydispersity and for three choices of the reduced temperature τ . We consider here constant stickiness coefficients (case IV) to allow a comparison with numerical work for discrete mixtures¹². It is gratifying that we find qualitatively the same trend, with the pressure decreasing with increasing polydispersity. Quantitatively, however, the results are not directly comparable because in Ref.¹² the less accurate compressibility (rather than energy) route was used to evaluate the pressure.

To interpret physically why the pressure decreases with polydispersity s at fixed packing fraction η , we note first that such a decrease is found also in the absence of adhesion (i.e. for HS). This has been established in simulations⁴⁰ and is reproduced qualitatively by the BMCSL equation of state; the intuitive reason is that in a fluid (gas or liquid) phase a spread of sizes allows for a more efficient packing of the particles. In such a less “jammed” particle arrangement one expects to find fewer interparticle contacts and so, in the presence of adhesion, fewer particle pairs interacting attractively. This will *increase* the pressure, counteracting the reduction, that one would expect for HS, resulting from the more efficient packing. Our results are quite consistent with this: at finite τ , we find that the pressure decreases *less* with polydispersity than in the HS limit $\tau \rightarrow \infty$.

The curves shown for the polydisperse cases in Fig. 4 cannot be used to infer phase coexistence properties directly by e.g. a Maxwell-construction: fractionation means that two coexisting phases do not have properties represented by a single relation between pressure and volume fraction. This remark holds true quite generally for single-phase equations of state in polydisperse systems, including e.g. the results obtained in Ref.¹² within the PY compressibility route to the equation of state. However, some more limited information on single-phase stability *can* be deduced. Specifically, a single phase cannot be stable where the pressure decreases with volume fraction. For the middle graph of Fig. 4, for example, where $\tau = 0.1186$ is just above the monodisperse critical point and so a monodisperse system is still stable at all densities, the polydisperse mixtures with $s = 0.2$ and 0.3 are already unstable in some range of densities. This means that the region where phase separation occurs must extend to larger values of τ for polydisperse than for monodisperse SHS, a result which – for case IV, as considered here – we will find confirmed very shortly.

We next turn to explicit results for the phase behaviour, starting in Fig. 5 with cases

II and IV for the stickiness coefficients, illustrated here for parent polydispersity $s = 0.3$. The cloud curve gives the boundary of the region where phase coexistence occurs. The shadow curve, which records the density of the coexisting phase at each point of incipient phase separation, is normally distinct from this. However, for the purely size-polydisperse cases considered here it is known on general grounds that when represented in terms of volume fraction rather than density the cloud and shadow curves *coincide* to $O(s^2)^{32,33}$. It is reassuring that, as Fig. 5 shows, this property is preserved by the PY approximation.

Turning to more detailed features of Fig. 5, we observe that in case IV the coexistence region is broadened towards both lower and higher volume fractions. As the monodisperse critical point is approached, the perturbation expansion breaks down as expected and the cloud/shadow curves diverge. No quantitative information can then be extracted in this regime, but the fact that the divergence is *outwards* still tells us that the coexistence region in the polydisperse case extends to *larger* values of τ than for monodisperse SHS. This is consistent with our inference from the single-phase equation of state above.

Comparing cases II and IV in Fig. 5 one sees first that the phase boundary shifts are rather smaller in the former than the latter. Also the (slight) broadening of the phase separation region towards lower η is now restricted to τ below around 0.093, while above the opposite trend is observed. The divergence of the curves at the monodisperse critical point is now *inwards* so that phase coexistence must terminate at a values of τ below the monodisperse τ_c .

Figure 6 shows the cloud and shadow curves for case V. We find that the shifts away from the monodisperse binodal are rather larger than in the previous two cases, and therefore show results for a smaller polydispersity $s = 0.2$, rather than for $s = 0.3$. Cloud and shadow curves no longer collapse, consistent with expectation as case V is not purely size-

polydisperse. The cloud curve shows that the coexistence region *narrows* in this case, except on the high-density branch for τ below ≈ 0.085 . The inward divergence of the cloud curve shows that the coexistence region also shrinks towards lower τ . The shadow phases are more dense throughout than the phases on the same branch of the cloud curve. Except for the last point, these trends agree with the non-perturbative results of Ref.¹⁸ derived within the C0 closure.

Case I, shown in Fig. 7, has even stronger polydispersity effects and we show predictions for a correspondingly smaller polydispersity $s = 0.1$. For τ not too far below the critical point the behaviour is otherwise qualitatively similar to case V; for lower τ the coexistence region is displaced towards lower rather than, as in case V, higher volume fractions. The shrinking of the coexistence region towards lower τ is again in qualitative agreement with results from the simpler C0 closure¹⁸.

Finally we turn to the phase behaviour predicted for the AO model with a small polymer-to-colloid size ratio $\xi/\sigma_0 = 0.1$ and polydispersity $s = 0.07$, as shown in Fig. 8. For this choice of ξ we have $\gamma \approx 3.97$ at the critical point of the monodisperse system, and the condition $\delta_i \sim s \ll 1/\gamma$ for the validity of the expansion in particle size of the stickiness coefficients ϵ_{ij} is reasonably well obeyed. Here the coexistence region is broadened in all directions by the introduction of polydispersity: towards low and high densities, and also towards larger values of τ . The shadow phases are again more densely packed than the analogous cloud phases.

We conclude this section by considering fractionation effects. These are illustrated in Fig. 9 for cases II and I, for a parent distribution of Schulz form and with values of the polydispersity s as in the corresponding Figs. 5 and 7. When phase separation is approached from low densities, a gas cloud phase with the parental size distribution coexists with an

infinitesimal amount of a liquid shadow phase with a different size distribution. At the high density boundary of the coexistence region, a liquid cloud phase similarly coexists with a distinct gas shadow phase. Fig. 9 shows that for case II the liquid phase contains more larger particles than the coexisting gas in both of these situations (and therefore presumably throughout the whole coexistence range of parent densities at the chosen τ). Case I exhibits the opposite behaviour: here the liquid phases contain more *smaller* particles than their coexisting gas counterparts.

To understand this difference between cases I and II, we return to Eq. (17). Consider the gas cloud point, where $\rho_0^{(1)}$ and $\rho_0^{(2)}$ are the densities of coexisting gas and liquid in the monodisperse system; Δa then is the difference in the values of a between gas and liquid. If this is positive, then Eq. (17) says that the liquid shadow has an enhanced concentration of larger particles. By reversing the role of the two densities one then sees easily that also at the liquid cloud point the liquid phase will contain more of the larger particles than the gas (shadow) phase. In summary, the liquid contains predominantly the larger particles if $\Delta a > 0$, and the smaller particles if $\Delta a < 0$. But from Eq. (27), $\Delta a = \Delta a_0 + \epsilon_{1a}\Delta a_1$ so that different choices of stickiness coefficients affect the direction and strength of fractionation only via ϵ_{1a} . The functions Δa_0 and Δa_1 are shown in Fig. 10 and are both positive; as a result, Δa is positive when $\epsilon_{1a} > -\Delta a_0/\Delta a_1$ and negative otherwise. The ratio occurring on the r.h.s. is almost constant and remains close to $1/3$ over a large range of τ , as the inset of Fig. 10 demonstrates. We can now rationalize the difference between cases I and II observed above: for case I, $\epsilon_{1a} = -1 < -1/3$, hence $\Delta a < 0$ and fractionation will enrich the liquid in small particles; for case II, $\epsilon_{1a} = 0 > -1/3$ and one has the opposite situation. Referring to Table I we also conclude that case IV will have the same fractionation behaviour as case II, while case V will produce the same “direction” of fractionation (smaller particles

in the liquid) as case I but with quantitatively weaker effects. In the AO case ϵ_{1a} depends on τ as discussed in Sec. IIIB but this effect turns out to be weak quantitatively, with (for $\xi/\sigma_0 = 0.1$) ϵ_{1a} ranging from ≈ 0.95 at the critical point to ≈ 1.24 at $\tau = 0.065$. Taking for simplicity $\epsilon_{1a} \approx 1$ one infers that fractionation effects will be qualitatively similar to cases II and IV, but quantitatively Δa will be larger by a factor of around 4. All of these conclusions can be confirmed by detailed examination of the explicit results for the various cases.

B. Other approximation schemes

Once one accepts the PY closure, the results shown above are exact in their treatment of polydispersity, certainly within the perturbative setting of weakly polydisperse mixtures. However, the PY closure itself – while more accurate than its competitors – does remain an approximation. It is therefore useful to compare with the predictions of other approximation schemes to assess the robustness of our predictions. We do this first for case II, where an approximate free energy of BMCSL type can be constructed, and then for the AO model, which can be analysed using the free volume theory of Refs.^{41,42}.

To construct the alternative approximation for case II one starts from a virial expansion of the excess free energy density up to the third virial coefficient. This is easily found as

$$f^{\text{ex}} = \rho\rho_3 + (3 - 12t)\rho_1\rho_2 + \frac{1}{2} [\rho\rho_3^2 + 3(1 - 12t + 48t^2 - 32t^3)\rho_2^3 + 6(1 - 4t)\rho_1\rho_2\rho_3] , \quad (28)$$

where $t = 1/(12\tau)$; the terms of second order in density agree with the energy route of the C0 approximation¹⁸. The interesting feature of this result is that the fourth order moment ρ_4 does not appear, in contrast to the analogous expansions for the other cases I, IV and V that we have considered. Furthermore, the only modification compared to the pure HS

case is in the t -dependence of the coefficients. These observations suggest that it should be possible to construct a modified free energy expression of BMCSL-type which matches the above virial expansion to third order in density. Remarkably, if the desired modified BMCSL form is parametrized in a fairly general manner as

$$f^{\text{ex}} = \left(A_1 \frac{\rho_2^3}{\rho_3^2} - A_2 \rho \right) [\ln(1 - D\rho_3) + E] + \frac{3B\rho_1\rho_2}{1 - D\rho_3} + \frac{C\rho_2^3}{\rho_3(1 - D\rho_3)^2} , \quad (29)$$

then by expanding to third order in density and matching to the expansion (28) one finds a *unique* solution for the coefficients:

$$E = 0 , \quad D = A_2 = 1 , \quad B = 1 - 4t , \quad C = A_1 = B^3 + 32t^3 .$$

The presence of polydispersity is crucial here: for a monodisperse system, the matching conditions to third order in density would not constrain the coefficients sufficiently.

One can now apply the perturbative scheme used throughout this paper to obtain from the excess free energy of Eq. (29) the functions a and b , and hence the cloud and shadow curves. (Note that the perturbative approach is used here mainly for ease of comparison with our other results; since the free energy (29) is truncatable, a full solution of the phase equilibrium conditions would be fairly straightforward.) The results are shown in Fig. 11; note that not just the polydisperse cloud/shadow curves but also the monodisperse binodal are different from the ones obtained from the PY approximation. Looking at the polydispersity-induced shifts, one sees that on the high-density branch of the cloud/shadow curve these are quite comparable to those from the PY approximation (Fig. 5), even semi-quantitatively. Polydispersity effects on the low-density branch are rather smaller, again as found within the PY closure. Near the critical point, however, the trends are reversed: the BMCSL-type approximation predicts an extension of the coexistence region towards larger τ and smaller η , whereas the PY approximation leads to the opposite result.

The second case where we have an alternative approximation scheme available for comparison is the AO model. The free volume theory of Ref.⁴¹ effectively linearizes the excess free energy in the polymer (reservoir) potential ρ_p , and the same is true for its generalization to polydisperse colloids⁴². It is therefore most accurate when the depletion interaction between the colloids, which is proportional to ρ_p , is small (in units of $k_B T$). In order to still get gas-liquid phase separation, the polymer size ξ must then not be too small. This is the opposite limit as for our SHS mapping, which will work best when $\xi \ll \sigma_0$ and the depletion attraction is large at contact. If anything one therefore expects the best agreement between the two approximations for intermediate values of ξ ; a suitable choice is $\xi/\sigma_0 = 0.1$ as investigated above. Fig. 12 compares the two sets of cloud and shadow curves predicted. On the vertical axis we plot the polymer (reservoir) volume fraction η_p . This equals $\rho_p \xi^3$ in our dimensionless units and is the conventional variable used in phase diagrams of colloid-polymer mixtures⁴¹. Comparison of the two panels of Fig. 12 reveals that the qualitative agreement between the two theories is surprisingly good. In particular, the qualitative changes caused by the presence of polydispersity (broadening of coexistence region to lower and higher colloid volume fraction and lower polymer volume fraction) are in full agreement. For the relevant range of polymer volume fractions there is even quite good quantitative agreement (though note the slightly different axis ranges on left and right), and the shifts of cloud and shadow curves away from the monodisperse binodal are also quite comparable. Even the predicted fractionation effects agree well: as the inset on the right of Fig. 12 demonstrates the calculated values of Δa are, apart from the slight shift in the critical point values of the polymer volume fraction, quite consistent with each other.

We note briefly that in order to calculate the free volume theory data shown in Fig. 12 we took the excess free energy for fully polydisperse colloids (at fixed polymer chemical

potential) derived in Ref.⁴² and then found the functions a and b by expanding explicitly as in Eq. (14). This gives for a the same result as obtained by Evans²², while b differs from his expression in terms of approximate correlation functions²². One might expect that our approach of deriving a and b from one unified polydisperse excess free energy would be somewhat more accurate than Evans' procedure of finding a and b by quite different routes. We have checked that for larger polymer sizes $\xi/\sigma_0 = 0.4$ our method predicts similar trends to those reported in²², but quantitatively the effects of polydispersity are less pronounced.

VI. CONCLUSIONS

We have presented a perturbative approach to the determination of the gas-liquid phase behaviour of polydisperse Sticky Hard Spheres (SHS), studied within the Percus Yevick (PY) integral equation theory. For arbitrary size polydispersity, the calculation of phase diagrams analogous to those reported here would normally require the solution of a large (or infinite) system of quadratic coupled equations, a task which in practice can be accomplished neither analytically nor numerically. To get around this bottleneck of the PY closure we focussed on weakly polydisperse mixtures, where the overall size distribution is narrow in the sense that its normalized (by the mean) standard deviation s is small compared to unity. This allowed us to calculate in closed form the leading order ($O(s^2)$) shifts of cloud and shadow curves away from the monodisperse binodal, and the corresponding fractionation effects. The thermodynamics was derived from the PY solution via the energy route because in the monodisperse case this method gives the best match to Monte Carlo simulation results, even for low reduced temperatures τ around and below the critical point.

In order to specify the properties of a SHS mixture one needs to know how the stickiness coefficients ϵ_{ij} depend on the sizes of the two interacting particles. We discussed a number

of plausible constraints on this size dependence. In obtaining explicit results we considered specifically the cases I-V (excluding III, which with our now more appropriate choice of reference length becomes identical to I) previously suggested within exact solutions of simpler closures like C0 and C1. Of these, cases II and IV are special since they can be seen as the sticky limit of purely size-polydisperse interactions, in which scaling of both particle sizes by a common factor only changes the range but not the strength of the interaction. We have also considered the AO model of a mixture of polydisperse colloids and polymers, which for small polymer size can be mapped to a good approximation onto an SHS model. The stickiness coefficients can be derived in this case rather than postulated; in contrast to the simpler ad hoc prescriptions of cases I-V, they are functions of τ .

In the simplest case IV of constant stickiness coefficients we first investigated the single-phase equation of state, finding qualitative agreement with a numerical solution of the compressibility equation of state for a small number of components by Robertus et al.¹². Moving on to phase coexistence proper, we found for cases II and IV that cloud and shadow curves coincide in the volume fraction representation and to $O(s^2)$, as expected on general grounds; less obviously our results also show that in these two cases the deviations of the polydisperse cloud/shadow curves away from the monodisperse binodal are quantitatively small. In all the other cases considered the shadow curves are located at higher volume fractions than the cloud curves, a trend observed in many other polydisperse systems^{22,29}.

Summarizing our findings regarding the effect of polydispersity on the extent of the coexistence region as delimited by the cloud curve, it is simplest initially to group the different scenarios according to their behaviour near the critical point. For case IV and the AO model (with a polymer-to-colloid size ratio of 0.1) the coexistence region is shifted to higher reduced temperatures τ ; conversely, at fixed τ it covers a wider range of parent

volume fractions η . Cases I, II and V, on the other hand, show the opposite behaviour, with the coexistence region shrinking towards lower τ .

The trends in cases IV and AO remain unchanged as one moves to lower values of τ , with the coexistence region continuing to broaden towards lower and higher values of η at the two ends (gas and liquid). In the other cases the shrinking trend near the critical point can be reversed at lower τ . E.g. for case II one also eventually sees a broadening to lower (gas branch) and higher (liquid branch) η . For case V the coexistence region is shifted to *higher* η at both ends (gas and liquid) at low τ ; case I shows the opposite behaviour.

We have analyzed also the fractionation effects that accompany polydisperse phase separation, where coexisting phases have different particle size distributions. Depending on the stickiness coefficients considered, the liquid phase contains predominantly the larger (as in cases II, IV and AO) or the smaller particles (as in cases I and V). We rationalized this result by showing that the fractionation effects depend on the stickiness coefficients only via the expansion coefficient ϵ_{1a} ; where this is above $\approx -1/3$, the larger particles accumulate in the liquid phase, otherwise in the gas.

Finally we have compared our results with the predictions from other available approximation schemes, to check their robustness. Case II is important here because a variety of simple but realistic interactions potentials, used in the literature to model short ranged attractions in real solutions of colloids, reverse micelles or globular proteins, can be mapped onto this model³⁴. We constructed an approximate excess free energy by allowing various coefficients within the BMCSL free energy for hard spheres to be τ -dependent and matching to the (for case II, particularly simple) third order virial expansion. The resulting binodal in the monodisperse limit is rather different from the one obtained from the PY closure with the energy route. The polydispersity-induced shifts of the (coincident)

cloud/shadow curves are nevertheless comparable to those predicted by our PY analysis, but only sufficiently far below the critical point. Near the critical point the BMCSL-like excess free energy predicts an enlargement of the coexistence region towards higher τ , while the PY closure gives the opposite result. Given that in the monodisperse case the PY binodal is rather closer to simulation results than the BMCSL-like one, we would expect that also for the polydispersity effects the PY predictions are more accurate.

The second model for which we considered an alternative approximation scheme was the AO model. Here a direct comparison with free volume theory is straightforward since for the latter a generalization to polydisperse colloids has recently been derived⁴². Even though one expects the two approaches to be valid in complementary regions (small polymer size ξ for the SHS mapping, larger ξ for free volume theory) we found very good qualitative and even semi-quantitative agreement of the predictions from the two routes for an intermediate value (0.1) of the polymer-to-colloid size ratio.

In future work, direct simulations of polydisperse SHS mixtures would obviously be of interest to test our predictions and resolve any differences with other approximation schemes, e.g. in case II. Simulations would be ideal here since in contrast to experiment they would allow one to probe directly different choices for the stickiness coefficients. Because of the presence of polydispersity, a grand canonical Monte Carlo approach^{32,43,44,45} may be the simulation method of choice, possibly supplemented by specific cluster algorithms tailored to sticky interactions^{19,20,21}. For the physically more realistic AO model, our predictions should be more accurate than those of free volume theory for small polymer-to-colloid size ratios. Detailed experimental or simulation tests in this regime would be welcome. In simulations one could work directly with the AO-depletion potential for the colloids, without ever representing the polymers explicitly. For comparison with experiment one would need to work out

the actual volume fraction of polymer in the system rather than in a reservoir; this should in principle be a straightforward exercise once our excess free energy has been rewritten as a function of polymer chemical potential. On the experimental side one would require that the colloids are sufficiently polydisperse (beyond a terminal polydispersity around $s = 0.07$; see the discussion and bibliography in Ref.⁴⁶) to suppress kinetically any solid phases, thus allowing stable observation of the gas-liquid phase splits we have calculated.

APPENDIX A: PERTURBATIVE EXPANSION OF L_{ij}

For the perturbative expansion of Eq. (18) one needs the expansions of α_{ij} , β_{ij} and ϕ_{ij} . These involve the trivial expansions

$$\sigma_i = 1 + \delta_i , \quad (\text{A1})$$

$$\sigma_{ij} = 1 + \frac{1}{2}(\delta_i + \delta_j) , \quad (\text{A2})$$

$$\sigma_i \sigma_j = 1 + (\delta_i + \delta_j) + \delta_i \delta_j . \quad (\text{A3})$$

One also needs the expansions to quadratic order of the moments

$$\rho_m = \rho \langle (1 + \delta)^m \rangle = \rho (1 + m \langle \delta \rangle + \frac{1}{2} m(m-1) \langle \delta^2 \rangle + \dots) , \quad (\text{A4})$$

giving in particular $\rho_2 = \rho(1 + 2\langle \delta \rangle + \langle \delta^2 \rangle)$ and $\Delta = 1 - \eta = 1 - \rho_3 = \Delta_0 - 3\rho \langle \delta \rangle - 3\rho \langle \delta^2 \rangle$ with $\Delta_0 = 1 - \rho$ as defined in the main text. The final ingredient is the expansion (6) for the ϵ_{ij} , which is left in general form to allow different possible choices of the stickiness coefficients to be considered together. Altogether one gets the following expansion coefficients for the

α_{ij} :

$$\alpha_0\tau = \frac{1}{\Delta_0} + \frac{3}{2}\frac{\rho}{\Delta_0^2} ,$$

$$\alpha_{1a}\tau = (1 + \epsilon_{1a})\frac{1}{\Delta_0} + \left(\frac{9}{4} + \frac{3}{2}\epsilon_{1a}\right)\frac{\rho}{\Delta_0^2} ,$$

$$\alpha_{1b}\tau = 6\frac{\rho}{\Delta_0^2} + 9\frac{\rho^2}{\Delta_0^3} ,$$

$$\alpha_{2a}\tau = \left(\frac{1}{2} + 2\epsilon_{1a} + \epsilon_{2a}\right)\frac{1}{\Delta_0} + \left(3 + \frac{9}{2}\epsilon_{1a} + \frac{3}{2}\epsilon_{2a}\right)\frac{\rho}{\Delta_0^2} ,$$

$$\alpha_{2b}\tau = \left(\frac{1}{4} + \epsilon_{1a} + \epsilon_{2b}\right)\frac{1}{\Delta_0} + \left(\frac{3}{4} + \frac{9}{4}\epsilon_{1a} + \frac{3}{2}\epsilon_{2b}\right)\frac{\rho}{\Delta_0^2} ,$$

$$\alpha_{2c}\tau = \left(\frac{15}{2} + 6\epsilon_{1a}\right)\frac{\rho}{\Delta_0^2} + \left(\frac{27}{2} + 9\epsilon_{1a}\right)\frac{\rho^2}{\Delta_0^3} ,$$

$$\alpha_{2d}\tau = 27\frac{\rho^2}{\Delta_0^3} + \frac{81}{2}\frac{\rho^3}{\Delta_0^4} ,$$

$$\alpha_{2e}\tau = \frac{9}{2}\frac{\rho}{\Delta_0^2} + 9\frac{\rho^2}{\Delta_0^3} .$$

Similarly one has for the β_{ij}

$$\beta_0\tau = \rho ,$$

$$\beta_{1a}\tau = \left(\frac{1}{2} + \epsilon_{1a}\right)\rho ,$$

$$\beta_{1b}\tau = 0 ,$$

$$\beta_{2a}\tau = (\epsilon_{1a} + \epsilon_{2a})\rho ,$$

$$\beta_{2b}\tau = \left(\frac{1}{2}\epsilon_{1a} + \epsilon_{2b}\right)\rho ,$$

$$\beta_{2c}\tau = 0 ,$$

$$\beta_{2d}\tau = 0 ,$$

$$\beta_{2e}\tau = 0 ,$$

and for the ϕ_{ij}

$$\phi_0 = \frac{1}{\Delta_0} ,$$

$$\phi_{1a} = \frac{1}{\Delta_0} ,$$

$$\phi_{1b} = \frac{3\rho}{\Delta_0^2} ,$$

$$\phi_{2a} = \frac{1}{\Delta_0} ,$$

$$\phi_{2b} = 0 ,$$

$$\phi_{2c} = \frac{3\rho}{\Delta_0^2} ,$$

$$\phi_{2d} = \frac{9\rho^2}{\Delta_0^3} ,$$

$$\phi_{2e} = \frac{3\rho}{\Delta_0^2} .$$

One now inserts these expansions into Eq. (18) and proceeds as explained in the main text to obtain the desired conditions on the expansions coefficients L_0, \dots, L_{2e} of the L_{ij} .

To state these, it is helpful to define the quantities

$$M_{\alpha,\beta} \equiv \frac{1}{12} L_\alpha L_\beta - \frac{1}{2} (L_\alpha \phi_\beta + L_\beta \phi_\alpha) ,$$

where Greek indices stand for the labels 0, 1a, 1b, 2a, 2c, 2d, 2e, of the coefficients of the

perturbative expansions. The desired conditions are then

$$L_0 = \alpha_0 + \beta_0 M_{0,0} , \quad (\text{A5})$$

$$L_{1a} = \alpha_{1a} + \beta_{1a} M_{0,0} + \beta_0 M_{0,1a} , \quad (\text{A6})$$

$$L_{1b} = \alpha_{1b} + \beta_{1b} M_{0,0} + 2\beta_0 (M_{0,1a} + M_{0,1b}) , \quad (\text{A7})$$

$$L_{2a} = \alpha_{2a} + \beta_{2a} M_{0,0} + 2\beta_{1a} M_{0,1a} + \beta_0 M_{1a,1a} , \quad (\text{A8})$$

$$L_{2b} = \alpha_{2b} + \beta_{2b} M_{0,0} + \beta_{1a} M_{0,1a} + \beta_0 M_{0,2b} , \quad (\text{A9})$$

$$\begin{aligned} L_{2c} = & \alpha_{2c} + \beta_{2c} M_{0,0} + 2\beta_{1a} (M_{0,1a} + M_{0,1b}) + \beta_{1b} M_{0,1a} \\ & + \beta_0 (M_{1a,1a} + M_{1a,1b} + M_{0,2a} + M_{0,2c}) , \end{aligned} \quad (\text{A10})$$

$$\begin{aligned} L_{2d} = & \alpha_{2d} + \beta_{2d} M_{0,0} + 2\beta_{1b} (M_{0,1a} + M_{0,1b}) \\ & + \beta_0 (2M_{0,2c} + 2M_{0,2d} + 2M_{1a,1b} + M_{1b,1b}) , \end{aligned} \quad (\text{A11})$$

$$L_{2e} = \alpha_{2e} + \beta_{2e} M_{0,0} + \beta_0 (M_{1a,1a} + 2M_{0,2b} + 2M_{0,2e}) , \quad (\text{A12})$$

The first of these determines L_0 and leads back to Baxter's solution (24) for the monodisperse case. All other equations involve the desired coefficient on the left at most linearly on the right hand side and so are trivial to solve; e.g. Eq. (A6) has $L_{1,a}$ on the left and implicitly via $M_{0,1a}$ on the right. Running through the equations in order, all expansion coefficients can then be found.

* Electronic address: rfantoni@unive.it

† Electronic address: gazzillo@unive.it

‡ Electronic address: achille@unive.it

§ Electronic address: peter.sollich@kcl.ac.uk

¹ H. Löwen, Phys. Rep. **237**, 249 (1994).

- ² G. Nägele, Phys. Rep. **272**, 215 (1996).
- ³ J. Lyklema, *Fundamental of Interface and Colloid Science* (Elsevier, 2005).
- ⁴ J. Lyklema, *Fundamental of Interface and Colloid Science* (Elsevier, 2000).
- ⁵ R. J. Baxter, J. Chem. Phys. **49**, 2770 (1968).
- ⁶ R. J. Baxter, in *Physical Chemistry, an Advanced Treatise*, vol. 8A, ed. D. Henderson (Academic Press, New York, 1971) ch. 4.
- ⁷ R. O. Watts, D. Henderson, and R. J. Baxter, Advan. Chem. Phys. **21**, 421 (1971).
- ⁸ R. J. Baxter, J. Chem. Phys. **52**, 4559 (1970).
- ⁹ B. Barboy, Chem. Phys. **11**, 357 (1975).
- ¹⁰ J. W. Perram and E. R. Smith, Chem. Phys. Lett. **35**, 138 (1975).
- ¹¹ B. Barboy and R. Tenne, Chem. Phys. **38**, 369 (1979).
- ¹² C. Robertus, W. H. Philipse, J. G. H. Joosten, and Y. K. Levine, J. Chem. Phys. **90**, 4482 (1989).
- ¹³ S. H. Chen, J. Rouch, F. Sciortino, and P. Tartaglia, J. Phys.:Condens. Matter **6**, 10855 (1994).
- ¹⁴ R. Piazza, V. Peyre, and V. Degiorgio, Phys. Rev. E **58**, R2733 (1998).
- ¹⁵ P. Prinsen and T. Odijk, J. Chem. Phys. **121**, 6525 (2004).
- ¹⁶ G. Stell, J. Stat. Phys. **63**, 1203 (1991).
- ¹⁷ D. Gazzillo and A. Giacometti, J. Chem. Phys. **120**, 4742 (2004).
- ¹⁸ R. Fantoni, D. Gazzillo, and A. Giacometti, J. Chem. Phys. **122**, 034901 (2005).
- ¹⁹ M. A. Miller and D. Frenkel, Phys. Rev. Lett. **90**, 135702-1 (2003).
- ²⁰ M. A. Miller and D. Frenkel, J. Chem. Phys. **121**, 535 (2004).
- ²¹ M. A. Miller and D. Frenkel, J. Phys. Cond. Mat. **16**, S4901 (2004).
- ²² R. M. L. Evans, J. Chem. Phys. **114**, 1915 (2001).

- ²³ R. Fantoni, D. Gazzillo, and A. Giacometti, Phys. Rev. E **72**, 011503 (2005).
- ²⁴ R. P. Sear, Mol. Phys. **96**, 1013 (1999).
- ²⁵ S. Auer and D. Frenkel, Nature **413**, 711 (2001).
- ²⁶ P. N. Pusey and W. van Megen, Phys. Rev. Lett. **59**, 2083 (1987).
- ²⁷ W. C. K. Poon, F. Renth, R. M. L. Evans, D. J. Fairhurst, M. E. Cates, and P. N. Pusey, Phys. Rev. Lett. **83**, 1239 (1999).
- ²⁸ Hans C. Andersen, John D. Weeks, and David Chandler, Phys. Rev. A **4**, 1597 (1971).
- ²⁹ P. Sollich, J. Phys. Cond. Matt. **14**, R79 (2002).
- ³⁰ P. Sollich and M. E. Cates, Phys. Rev. Lett. **80**, 1365 (1998).
- ³¹ P. Sollich, P. B. Warren, and M. E. Cates, Adv. Chem. Phys. **116**, 265 (2001).
- ³² N. B. Wilding, M. Fasolo, and P. Sollich, J. Chem. Phys. **121**, 6887 (2004).
- ³³ P. Sollich (2006), unpublished.
- ³⁴ D. Gazzillo, A. Giacometti, R. Fantoni, and P. Sollich (2006), unpublished.
- ³⁵ S. Asakura and F. Oosawa, J. Chem. Phys. **22**, 1255 (1954).
- ³⁶ J. L. Barrat and J. P. Hansen, *Basic Concepts for Simple and Complex Liquids* (Cambridge, 2003).
- ³⁷ T. Boublík, J. Chem. Phys. **53**, 471 (1970).
- ³⁸ G. A. Mansoori, N. F. Carnahan, K. E. Starling, and T. W. Leland Jr., J. Chem. Phys. **54**, 1523 (1971).
- ³⁹ Note that the energy route to the equation of state of HS fluids is ill defined since the internal energy is just that of the ideal gas. So in the PY approximation one could use⁴⁷ either the compressibility pressure $P^{\text{PY(c)}}$ or the virial pressure $P^{\text{PY(v)}}$. For a mixture of a discrete number of species it is known that the BMCSL pressure $P^{\text{BMCSL}} = (2P^{\text{PY(c)}} + P^{\text{PY(v)}})/3$ is more accurate

than either of these two limits. Recently, the equivalence between the energy and virial routes to the equation of state for the one-component HS fluid has been shown in⁴⁸. We use the BMCSL expression throughout, except in figure 1 where the PY compressibility pressure is used for ease of comparison with earlier work¹⁸.

- ⁴⁰ S. E. Phan, W. B. Russel, J. X. Zhu, and P. M. Chaikin, J. Chem. Phys. **108**, 9789 (1998).
- ⁴¹ H. N. W. Lekkerkerker, W. C. K. Poon, P. N. Pusey, A. Stroobants, and P. B. Warren, Europhys. Lett. **20**, 559 (1992).
- ⁴² M. Fasolo and P. Sollich, J. Chem. Phys. **122**, 074904 (2005).
- ⁴³ N. B. Wilding and P. Sollich, J. Chem. Phys. **116**, 7116 (2002).
- ⁴⁴ N. B. Wilding and P. Sollich, Europhys. Lett. **67**, 219 (2004).
- ⁴⁵ N. B. Wilding, P. Sollich, and M. Fasolo, Phys. Rev. Lett. **95**, 155701 (2005).
- ⁴⁶ M. Fasolo and P. Sollich, Phys. Rev. E **70**, 041410 (2004).
- ⁴⁷ J. J. Salacuse and G. Stell, J. Chem. Phys. **77**, 3714 (1982).
- ⁴⁸ A. Santos, J. Chem. Phys. **123**, 104102 (2005).

LIST OF FIGURES

Fig. 1 Equation of state, from the energy route, for a one-component fluid of SHS. From left to right and top to bottom the four panels refer respectively to a reduced temperature of $\tau = 1.00, 0.50, 0.20$, and 0.15 . The continuous line corresponds to the MSA approximation, the dotted line to the mMSA approximation, the short dashed line to the C1 approximation, the long dashed line to the PY approximation, the dot-dashed line to the WCA first order perturbation theory, squares to the WCA second order perturbation theory (with error bars indicating the range where the true value should lie with probability 99.7%), and triangles to the MC simulations of Miller and Frenkel²⁰. In all cases the HS component of the pressure was chosen to be the one obtained from the compressibility route of the PY approximation³⁹.

Fig. 2 The overlap volume $\mathcal{V}_{ov}(r)$ of the two exclusion zones around colloid particles of diameter σ_i and σ_j which cannot be accessed by polymers of diameter ξ .

Fig. 3 Phase diagram of the monodisperse SHS fluid obtained with the PY closure and the energy route to thermodynamics. Shown are the binodal and spinodal curves and the region where the PY equation has no solution (see Eq. (25)).

Fig. 4 Pressure from the energy route of the PY approximation for a single (parent) phase with case IV stickiness coefficients, plotted against volume fraction. Results are shown for several small values of the polydispersity s (see legend) and well above, just above, and below (from left to right) the critical point of the monodisperse system. The pressure was determined using Eq. (9) of Ref.²².

Fig. 5 Cloud and shadow curves for SHS mixtures with polydispersity $s = 0.3$, as obtained within the PY approximation and the energy route to thermodynamics, for coefficients

ϵ_{ij} chosen according to cases II and IV from Eq. (5). The shifts from the binodal of the monodisperse system (labeled “mono”) were calculated using Eq. (15) and give the leading ($O(s^2)$) corrections in a perturbative treatment of polydispersity. Note the collapse of the cloud and shadow curve, as expected to this order of the perturbation theory for purely size-polydisperse models^{32,33}, and the divergence of the perturbation theory at the monodisperse critical point.

Fig. 6 Cloud and shadow curves for the SHS model with polydispersity $s = 0.2$ and case V stickiness coefficients. The binodal of the monodisperse system is shown for comparison.

Fig. 7 Cloud and shadow curves for the SHS model with polydispersity $s = 0.1$ and case I stickiness coefficients. The binodal of the monodisperse system is shown for comparison.

Fig. 8 Cloud and shadow curves for the AO model with polymer-to-colloid size ratio $\xi/\sigma_0 = 0.1$ and (colloid) polydispersity $s = 0.07$. The binodal of the monodisperse system is shown for comparison.

Fig. 9 Fractionation in SHS mixtures with stickiness coefficients chosen according to cases II and I, at $\tau = 0.11$ and for polydispersities s as in the corresponding Figs. 5 and 7. Shown are the cloud (parent) size distribution $p(\sigma)$, taken to be of Schulz form, and the size distributions in the liquid shadow and gas shadow phases that form when coexistence is approached from low densities (gas cloud phase) and high densities (liquid cloud phase), respectively. For case II (main graph) the larger particles tend to accumulate in the liquid phase, while for case I (inset) the opposite is true.

Fig. 10 Decomposition $\Delta a = \Delta a_0 + \epsilon_{1a}\Delta a_1$ of the difference in a between gas and liquid phases. The two contributions Δa_0 and Δa_1 are plotted separately against τ ; the latter quantity is graphed on the vertical rather than the horizontal axis for ease of comparison with Figs. 5 to 8. Inset: Ratio $\Delta a_0/\Delta a_1$.

Fig. 11 Cloud and shadow curves for case II stickiness coefficients and with polydispersity $s = 0.3$, calculated using the BCMSL-type free energy, Eq. (29), rather than the PY approximation as in Fig. 5. The binodal of the monodisperse system, which differs from the PY result, is shown for comparison. Main graph: region around the critical point. Inset: global view of the results on the same scale as in Fig. 5.

Fig. 12 Comparison of predictions for AO model with polymer-to-colloid size ratio $\xi/\sigma_0 = 0.1$. Left: Results of SHS mapping analysed within PY approximation; as in Fig. 8 cloud and shadow curves are shown for colloid polydispersity $s = 0.07$, along with the monodisperse binodal for comparison. The vertical axis now shows the polymer volume fraction rather than the reduced temperature τ . Right: Analogous results obtained from free volume theory. Inset right: Fractionation coefficient Δa for the two approximation schemes.

LIST OF TABLES

Tab. 1 Coefficients of the perturbative expansion (6) of the adhesion parameters ϵ_{ij} for the four cases listed in Eq. (5).

	Case I	Case II	Case IV	Case V
ϵ_0	1	1	1	1
ϵ_{1a}	-1	0	0	-1/2
ϵ_{2a}	3/2	1/2	0	1/2
ϵ_{2b}	3/4	-1/4	0	1/4

TABLE I:

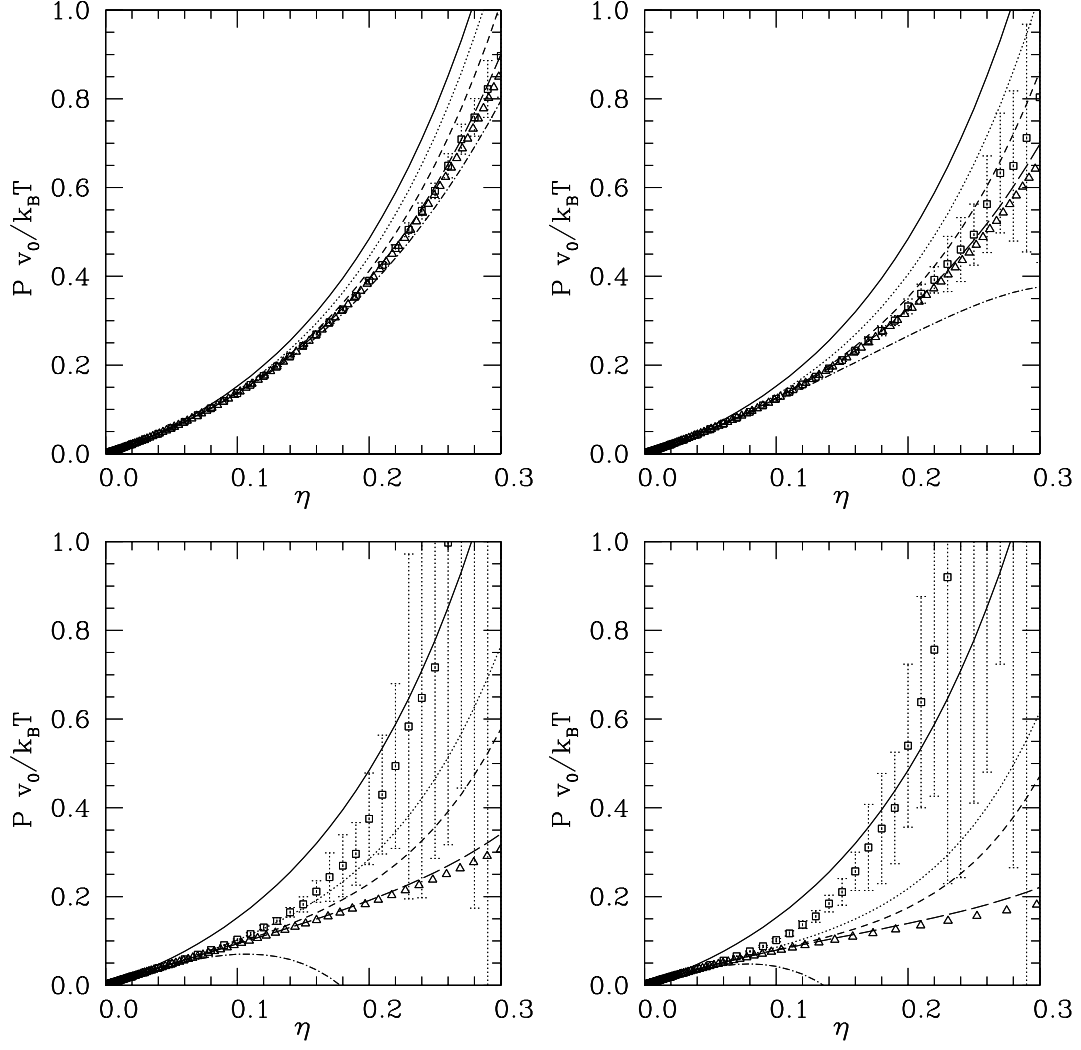


FIG. 1:

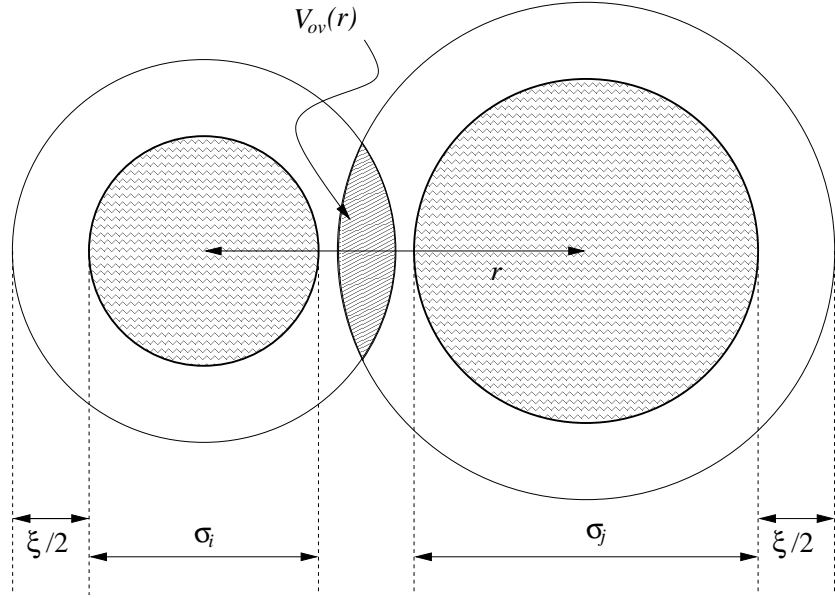


FIG. 2:

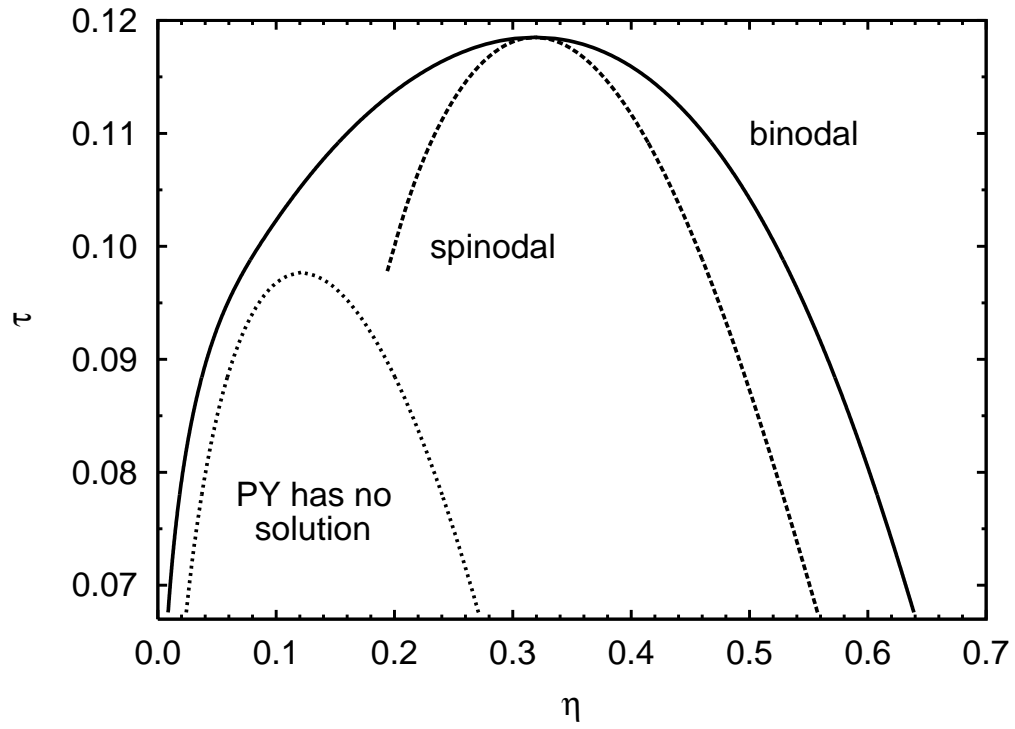


FIG. 3:

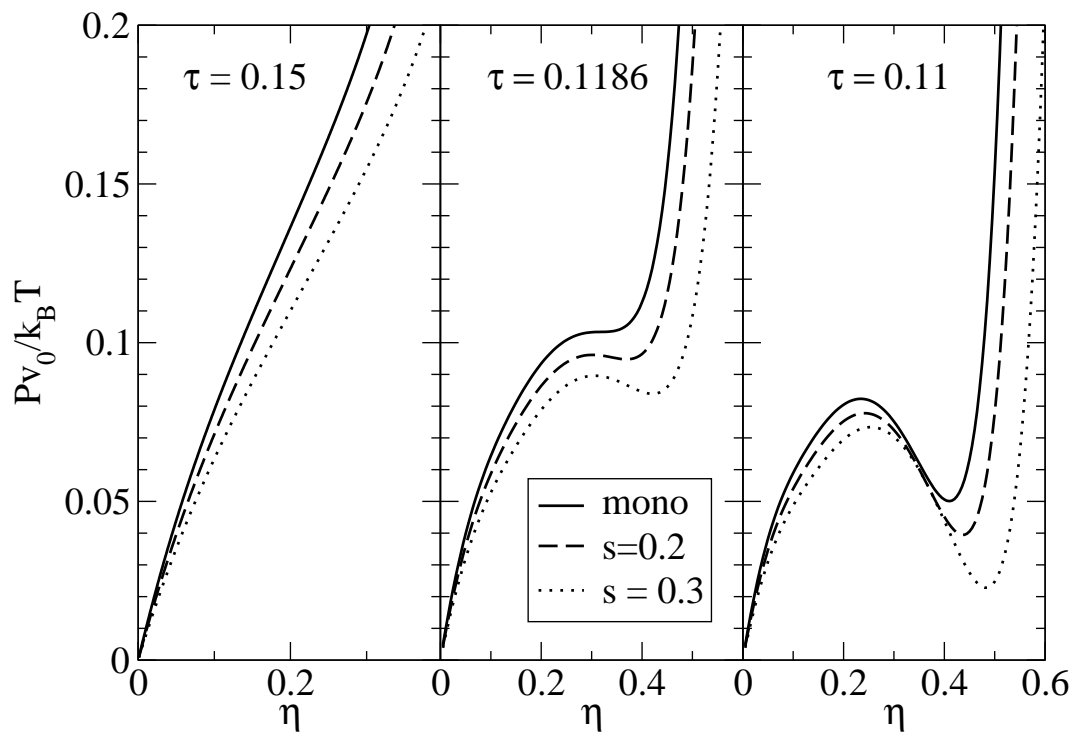


FIG. 4:

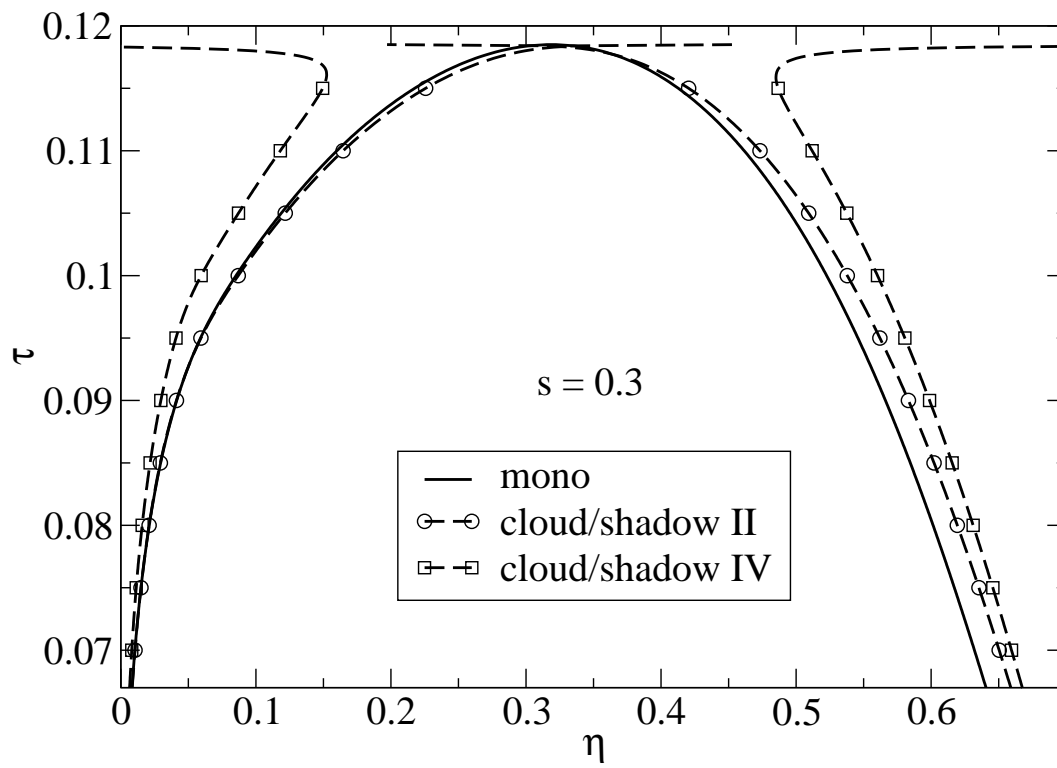


FIG. 5:

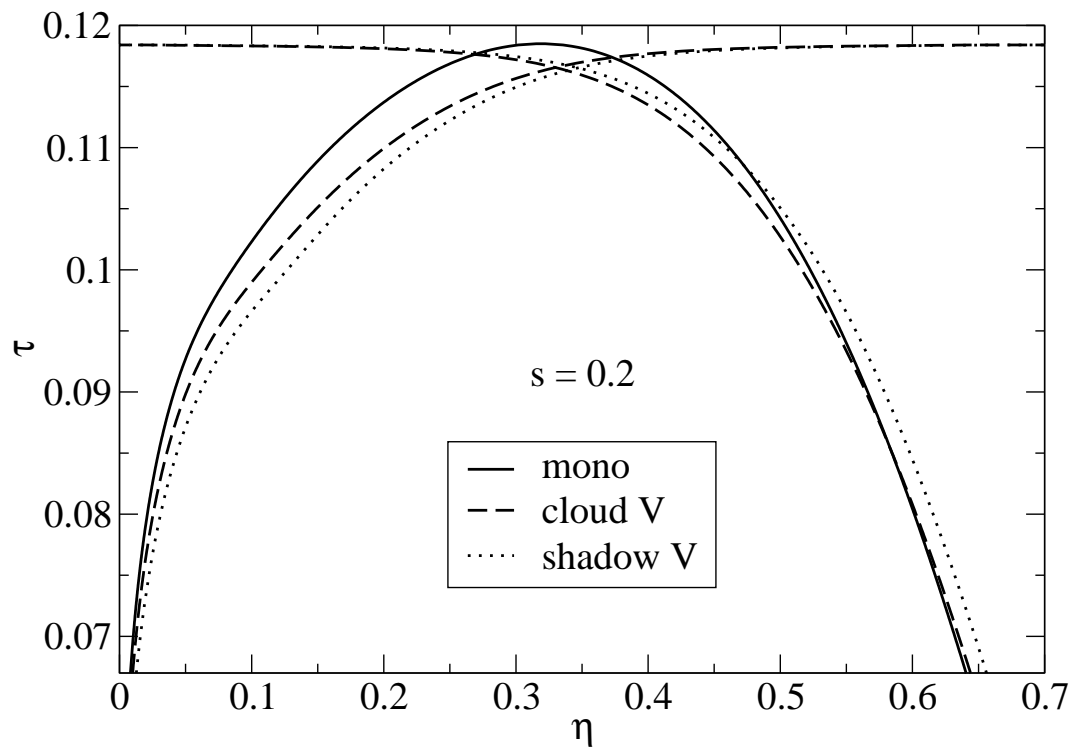


FIG. 6:

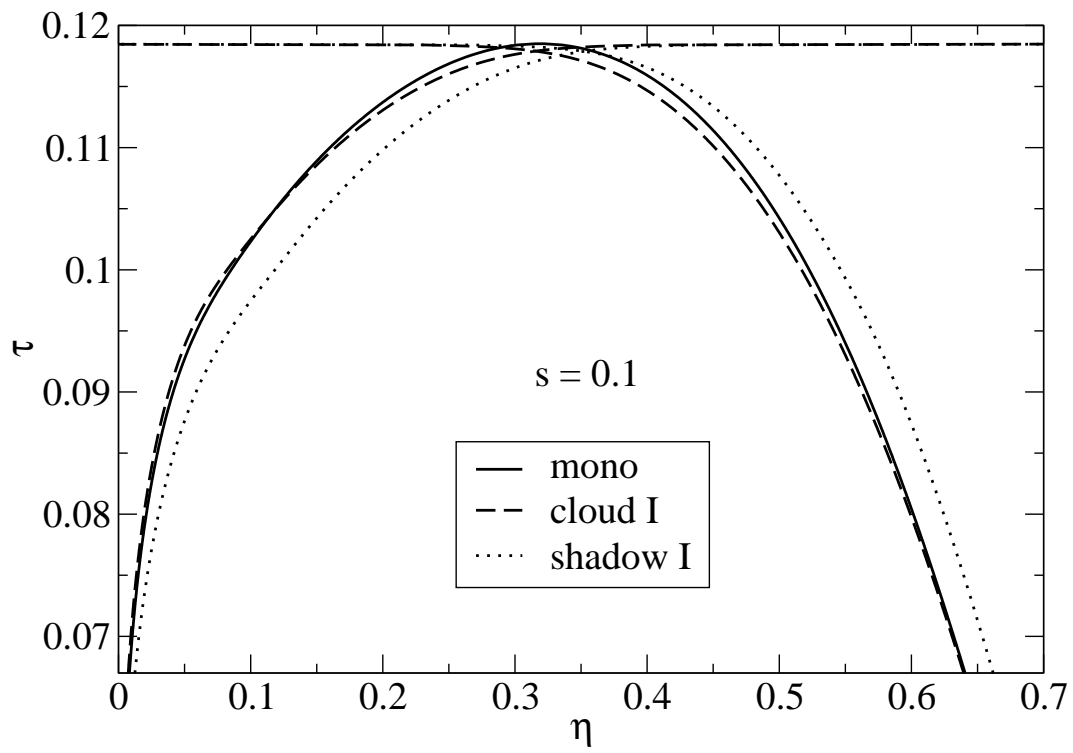


FIG. 7:

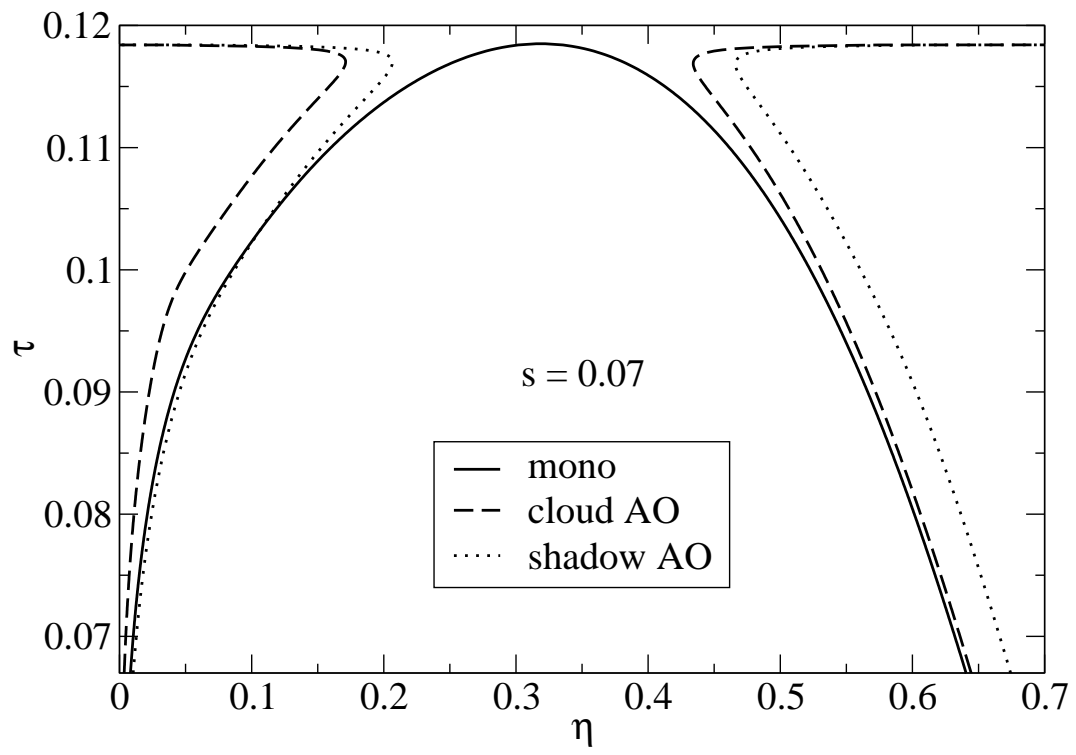


FIG. 8:

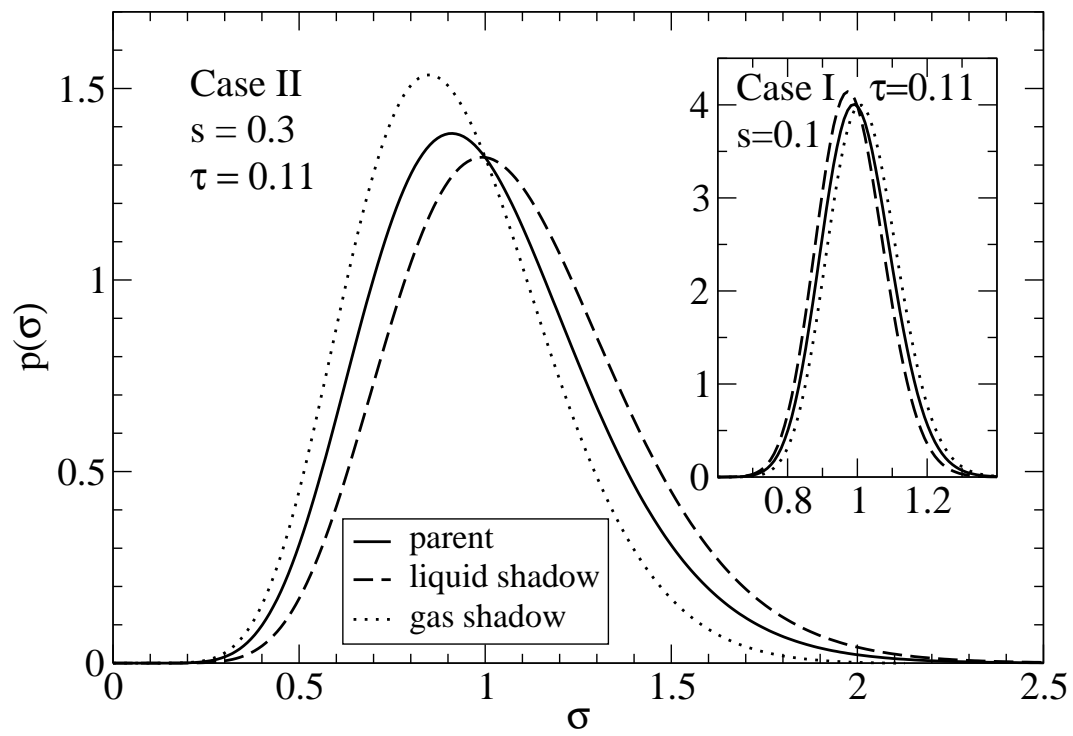


FIG. 9:

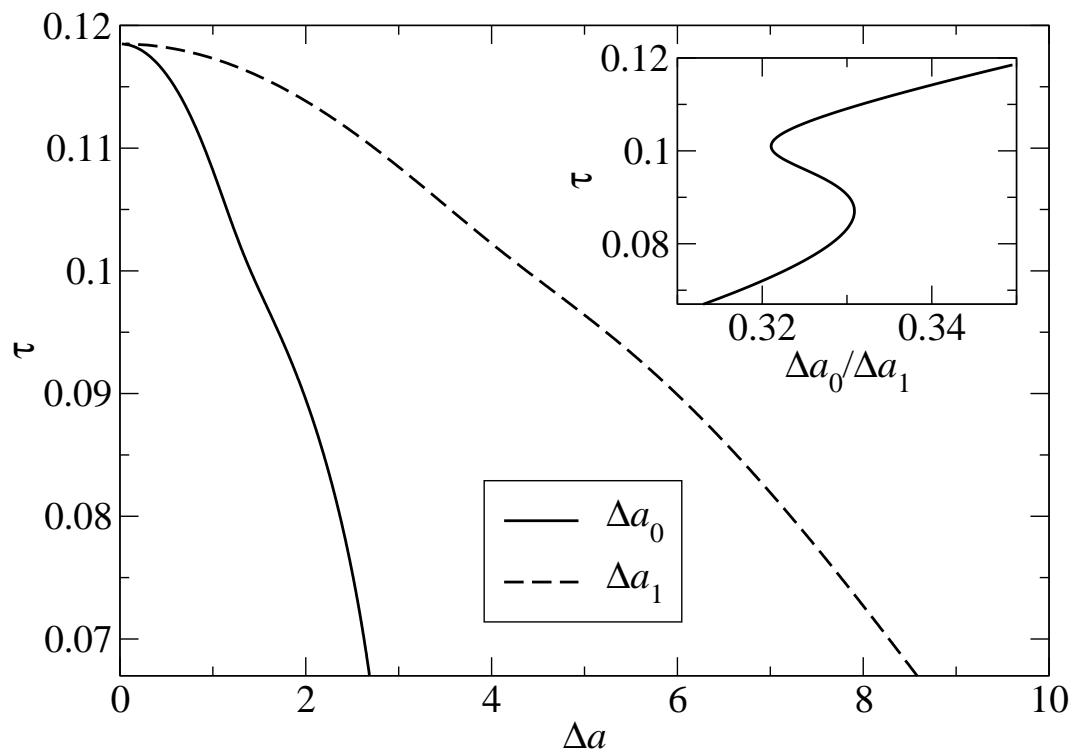


FIG. 10:

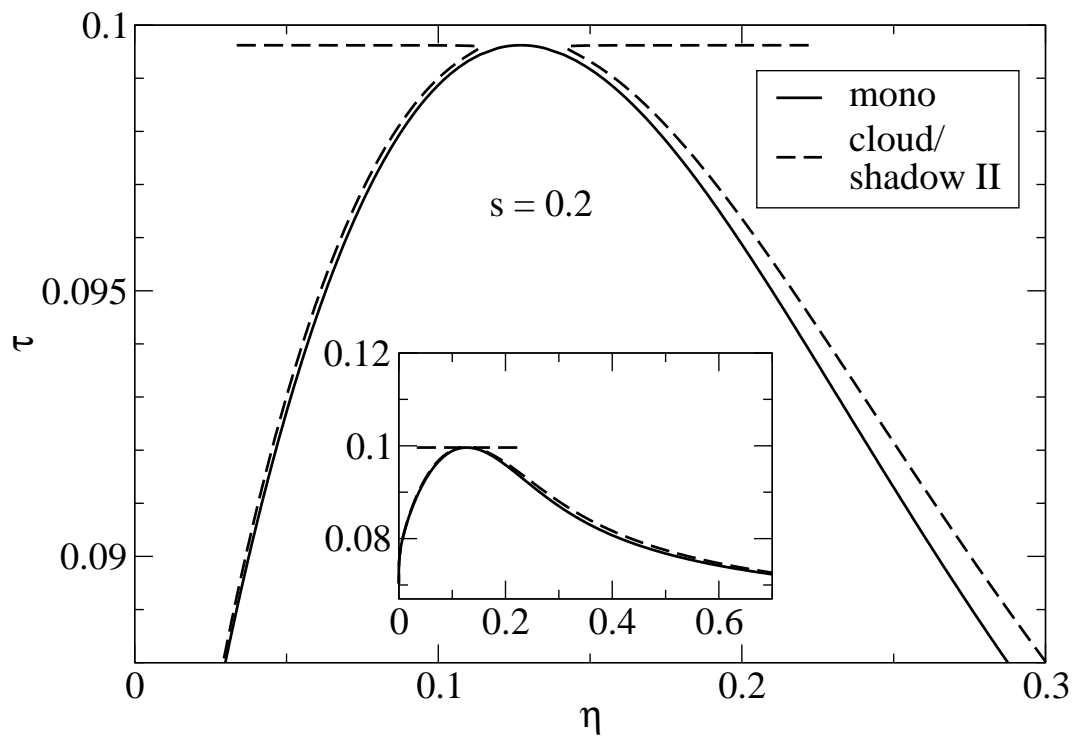


FIG. 11:

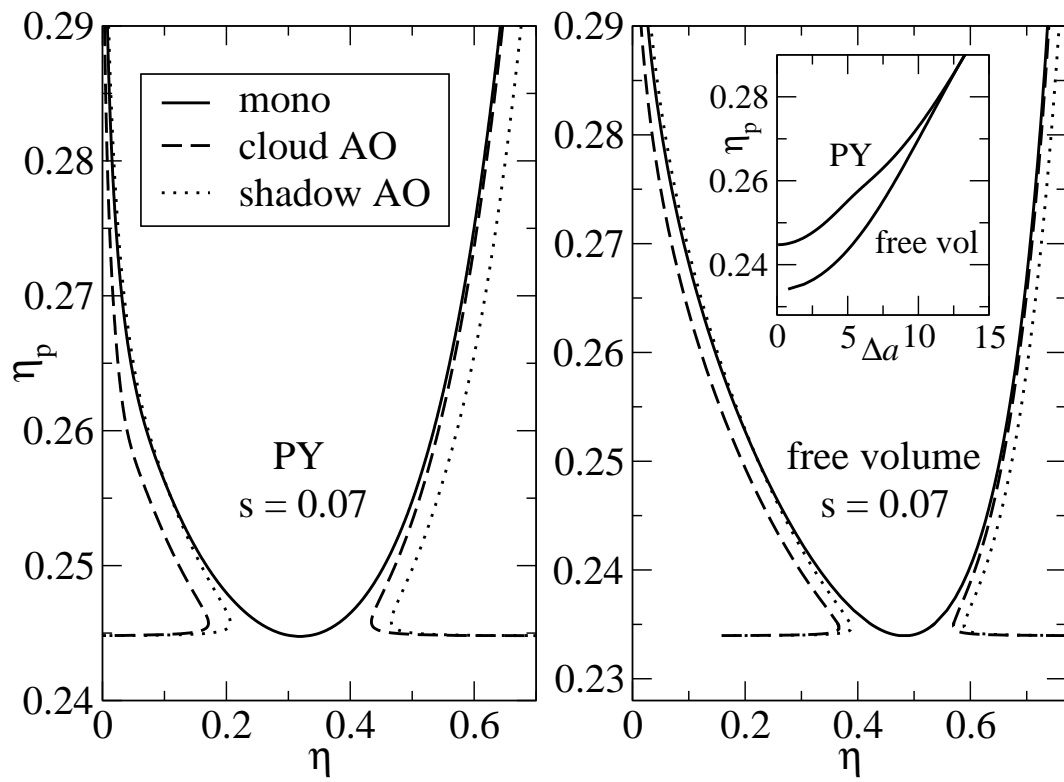


FIG. 12: